## Fe<sub>3</sub>O<sub>4</sub>@SiO<sub>2</sub> Magnetic Nanoparticles Modified with Cysteine: a New Adsorbent for Environmentally Friendly Adsorption/Desorption of Pb(II) ions

Yuanjing Bi<sup>1</sup>, Ningyan Sun<sup>1</sup>, Ailin Fan<sup>1</sup>, Ming Zhang<sup>2</sup>, Xiangming Liu<sup>3</sup>, Bo Xu<sup>1</sup>, Guihong Lan<sup>1</sup>, Haiyan Qiu<sup>4</sup>,\*

<sup>1</sup>College of Chemistry and Chemical Engineering, Southwest Petroleum University (SWPU), Chengdu 610500, China

<sup>2</sup>China Railway Water Group Co., Ltd., Xi'an 710000, China
 <sup>3</sup>Yin Chuan China Railway Water Group Co., LTD., Yinchuan 750000, China
 <sup>4</sup>Southwest Petroleum University, Chengdu, Sichuan 610500, China

#### **Abstract**

In recent years, nanoparticles have become the focus of scientific research because of their wide potential application value. Iron oxides show incredible magnetic saturation, stability, and intuitive properties on the surface, making them ideal for a variety of uses. In this paper, nanometer iron oxide particles are synthesized by co-deposition method, and silica is further used to avoid agglomeration. Functional synthesis of cysteine nanoparticles (FNMs-Cys). The optimum synthesis conditions and adsorption conditions were determined by orthogonal experiments. In addition, the anti-interference and regeneration cycle performance of FNMs-Cys are discussed. The samples were characterized by scanning electron microscope (SEM), X-ray diffractometer (XRD), Fourier transform infrared spectrometer (FTIR), N2 adsorption and desorption automatic specific surface and porosity analyzer (BET), thermogravimetric analysis (TG) and hysteresis loop test (VSM). The adsorption process of Pb2+ by FNMs-Cys accords with quasi-second-order kinetics and Langmuir isothermal adsorption model, which shows that the adsorption is mainly through chemical adsorption of monolayer, In the Langmuir model, the maximum single-layer adsorption capacity of FNMs-Cys for Pb2+ reached 174.85 mg/g. After five cycles of adsorption-desorption regeneration, FNMs-Cys still showed good stability and recyclability. At present, it is of forward-looking significance to study the removal effect of Pb2+ in water by using amino acid modified mesoporous magnetic silica materials in laboratory.

## **Keywords**

Cysteine; Mesoporous Silica; Adsorption; Heavy Metal Ions.

#### 1. Introduction

Heavy metal ion pollution is one of the major environmental problems facing water systems in the world. Among these heavy metal species, lead is a common pollutant due to its high toxicity, carcinogenicity, mutagenicity and wide range of industrial applications. Unlike organic pollutants, lead can not be biodegraded, but can also accumulate through the food chain, affecting the brain and nervous system of animals and causing irreversible organ damage. Therefore, it is very important to treat heavy metal wastewater. [1] At present, the treatment methods of heavy metal wastewater include chemical precipitation [2], ion exchange [3], membrane separation [4] and adsorption [5]. Adsorption has become a cost-effective method for pollutant removal [6]. Several sorbents such as natural zeolite [7], sodium alginate [8], and

chitosan [9], have been used to remove heavy metal ions from wastewater. However, the adsorption capacity of these materials is low and/or inefficient, and the process of separating the adsorbent from the aqueous solution after saturated adsorption is often complex and time consuming.

Fortunately, under a certain magnetic field, magnetic assisted chemical separation is an effective method to remove heavy metals from aqueous solutions. Magnetic nanoparticles, especially Fe<sub>3</sub>O<sub>4</sub> nanoparticles, have gained more and more attention due to their unique magnetic properties and preparation feasibility [10-11]. However, there are two major challenges. One is related to the reunion, poor dispersion of Fe<sub>3</sub>O<sub>4</sub> in water [12]. The other is the easy oxidation/dissolution of iron nanoparticles, especially at high concentrations of acid solution [13]. To solve these problems, a suitable shell structure or decorative material is usually introduced, and silica is known to be one of the ideal coatings for magnetic Fe<sub>3</sub>O<sub>4</sub> nanoparticles due to its reliable chemical stability, biocompatibility, and easy surface modification [14][15]. It was shown that after saturation adsorption, magnetic Fe<sub>3</sub>O<sub>4</sub>-SiO<sub>2</sub> composite particles can be easily separated from the mixed solution by an external magnetic field, And the adsorption effect of the material can be improved to some extent. For example, Vojoudi et al [16].investigated the adsorption of magnetic Fe<sub>3</sub>O<sub>4</sub>-SiO<sub>2</sub> composite particles on Pb(II) and Hg(II) and found that the composite particles had a strong adsorption capacity, with the maximum removal of Hg(II), Pb(II)) of 98.8% and 95.7%. In addition, L-cysteine[17][18] is a biocompatible, safe and non-toxic water-soluble amino acid that can be found in most highprotein foods, including animal sources (e.g., pork, dairy) or plant sources (e.g., broccoli, onion, garlic), has three functional groups (-SH,-NH<sub>2</sub>,-COOH), and possesses strong metal chelating ability. Some recent studies have reported that -SH,-NH2 functional groups can form crosslinked networks with epoxy groups to provide chemical stability and surface properties [19], and -SH,-NH<sub>2</sub>,-COOH can provide good biocompatibility and stability, and are well involved in the removal of metal ions from aqueous solutions by forming various complexes and thus [20]. Therefore, the introduction of cysteine would be a good choice.

Based on this background, in this paper, magnetic mesoporous silica microspheres (FNMs-Cys) with magnetic response were prepared by combining Fe<sub>3</sub>O<sub>4</sub> nanoparticles with silica and surface modifying them using cysteine, and magnetic mesoporous silica microspheres (FNMs-Cys) modified by cysteine were prepared. To evaluate the treatment effect of FNMs-Cys as adsorbent on simulated lead wastewater and its feasibility in practical application.

#### 2. Materials and Methods

#### 2.1. Chemicals and Materials

Ferrous sulfate heptahydrate, ferric chloride,ethyl orthosilicate (TEOS), cetyltrimethyl ammonium bromide (CTAB), 3-aminopropyl triethoxysilane (APTES), sodium borohydride, ammonia water, acetone, glutaraldehyde, purchased from Shanghai Maclin Biochemical Technology Company;L-cysteine, anhydrous ethanol, sodium nitrate, magnesium nitrate, ferric nitrate, sodium hydroxide, potassium hydroxide, hydrochloric acid, purchased from Chengdu Kelong Chemical Reagent Factory. The solutions were prepared with deionized water.

# 2.2. Synthesis of Aminosilanized Silica-coated Magnetite Nanomaterials Fe<sub>3</sub>O<sub>4</sub>@nSiO<sub>2</sub>@mSiO<sub>2</sub>-NH<sub>2</sub>

The synthesis of the absorbent was carried out via four defined steps. An illustration of the procedure is shown in Fig.1 After being magnetically separated via an external magnetic field, dry and set aside. Magnetic mesoporous silica was prepared by StÖber process [21].1g Fe<sub>3</sub>O<sub>4</sub>, 4 mL ammonia water, 80 mL ethanol, 20mL deionized water and 3 mL TEOS were stirred at room temperature for 2 h. The solid product was collected by a magnet and repeatedly washed with

a large amount of deionized water and absolute ethanol and dried under vacuum at 60  $^{\circ}$ C for 12h to obtain Fe<sub>3</sub>O<sub>4</sub>@nSiO<sub>2</sub> (Fe<sub>3</sub>O<sub>4</sub>-SiO<sub>2</sub>)magnetic particles. The washed microspheres were dispersed in a mixture of 100 mL deionized water containing ethanol (V ethanol: V water = 3: 4) Add 1 g CTAB, 4 mL ammonia water and 4 mLTEOS stir at room temperature for 6 h. Magnetite particles were collected with a magnetic bar and the templating agent CTAB was removed with acetone, then washed several times with distilled water and dried at 45  $^{\circ}$ C for 8 h to obtain Fe<sub>3</sub>O<sub>4</sub>@nSiO<sub>2</sub>@mSiO<sub>2</sub> (FNMs) samples.1g FNMs was dispersed in 50 mL ethanol solution, followed by ultrasonic dispersion for 30 min and adding 4 mL APTES and appropriate amount of ammonia water. After continuous agitation at 40  $^{\circ}$ C for 4 h, After completion of the reaction, the mixture was cooled to room temperature. The solid product was collected with a magnet, washed repeatedly with large amounts of deionized water and anhydrous ethanol, and dried under vacuum at 45  $^{\circ}$ C for 8 h to obtain the materialFe<sub>3</sub>O<sub>4</sub>@nSiO<sub>2</sub>@mSiO<sub>2</sub>-NH<sub>2</sub> (FNMs-NH<sub>2</sub>).

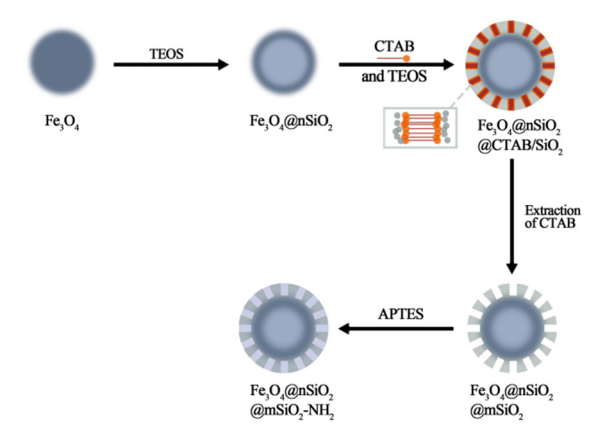


Fig 1. Schematic synthesis of magnetite nanomaterials coated with aminosilanized silica

# 2.3. Synthesis and Optimization of Magnetic Mesoporous Silica Modified with Cysteine

In the process of cysteine functional modification of magnetic mesoporous silica, glutaraldehyde is used as a crosslinking agent to connect FNMs-NH $_2$  and cysteine to obtain cysteine-functionalized magnetic mesoporous silica FNMS-Cys. The reaction equation of cysteine modified magnetic mesoporous silica is shown in Fig 2.In order to obtain the best modified composite, four factors and three levels orthogonal experiments were designed to explore the effects of pH, the ratio of m(FNMs-NH $_2$ ): m (cysteine), the amount of glutaraldehyde and the reaction temperature on the adsorption of Pb $_2$ + by the composite. The optimized conditions with the highest adsorption capacity were selected for subsequent experiments.

Fig2. Reaction equation of magnetic mesoporous silica modified by cysteine

#### 2.4. Characterizations of FNMs-Cys

The pore structure and surface morphology of Fe<sub>3</sub>O<sub>4</sub>, Fe<sub>3</sub>O<sub>4</sub>-SiO<sub>2</sub>, FNMs-NH<sub>2</sub> and FNMs-Cys were observed by scanning electron microscope (ZEISS Gemini 300). The element distribution of FNMs-Cys and FNMs-Cys-Pb (FNMs-Cys after Pb<sup>2+</sup> adsorption) was analyzed by Energy

Dispersive X-ray spectrometer (X-Max 50, Oxford instruments type). The surface functional groups of Fe<sub>3</sub>O<sub>4</sub>, Fe<sub>3</sub>O<sub>4</sub>-SiO<sub>2</sub>, FNMs-NH<sub>2</sub> and FNMs-Cys were determined by Fourier Transform infrared spectrometer (Tensor 27) in the spectral range of 4000-400cm<sup>-1</sup>. The crystalline structures of Fe<sub>3</sub>O<sub>4</sub>, Fe<sub>3</sub>O<sub>4</sub>-SiO<sub>2</sub>, FNMs-NH<sub>2</sub>, FNMs-Cys and FNMs-Cys-Pb were characterized by X-ray powder diffractometer (X 'Pert PRO).

## 2.5. Batch Adsorption Performance Experiment.

Batch experiments were carried out in this part to explore the effects of pH, FNMs-Cys addition amount, initial concentration, temperature and adsorption time on the adsorption effect of FNMs-Cys on Pb<sup>2+</sup>. The pH gradient was set as  $1\sim7$ , adsorbent dosage as  $0.2\sim1g/L$ , the temperature as  $10\sim50\,^{\circ}$ C, the adsorption time as  $0.5\sim12$ h, and the initial concentration as  $10-180\,\text{mg/L}$ . After shaking for  $10\,\text{h}$  at  $200\,\text{rpm}$  and  $25\,^{\circ}$ C, the concentration of Pb<sup>2+</sup> before and after adsorption in the solution was measured, and the optimal conditions were determined according to the calculated adsorption amount. The mass concentration of Pb<sup>2+</sup> before and after adsorption was determined by atomic absorption spectrophotometer, and the data were the average values of three repeated experiments.

## 2.6. Research on Regeneration Performance

In order to evaluate the possibility of regeneration and recycling of FNMs-Cys, adsorption-desorption experiments were carried out. Determine whether FNMs-Cys can exist stably in strong acidic media. Therefore, it was washed in 25 mL 0.01mol /L, 0.02mol /L, 0.05mol /L, 0.1mol /L and 0.2mol /L HCl solution with concentration gradient. At the same time, attention should be paid to whether the duration of washing FNMs-Cys in HCl solution will affect the desorption degree of FNMs-Cys. Set the washing time gradient to 10min, 20min, 30min, 50min, and 60min. The adsorption and desorption of FNMs-Cys (FNMs-Cys-Pb) composite material after Pb<sup>2+</sup> adsorption were carried out. The material was recycled for 5 times, and the experimental process was repeated for 4 times.

#### 2.7. Evaluation of Anti-interference Capability

In the lead-containing wastewater in real life, Pb<sup>2+</sup> does not exist alone, and there are many cations and anions coexisting. In this part, by adding the nitrates of Na<sup>+</sup>, K<sup>+</sup>,Ca<sup>2+</sup> and Mg<sup>2+</sup> with the same concentration gradient to form a binary system with Pb<sup>2+</sup>, the interference ability of Ca<sup>2+</sup>, Mg<sup>2+</sup>, Na<sup>+</sup> and K<sup>+</sup> on the adsorption of Pb<sup>2+</sup> by FNMs-Cys was explored. At the same time, six representative anions were selected, namely Cl<sup>-</sup>, NO<sub>3</sub><sup>-</sup>, Br<sup>-</sup>, SO<sub>4</sub><sup>2-</sup>, CO<sub>3</sub><sup>2-</sup> and F<sup>-</sup>, and six sodium salts of NaCl, NaNO<sub>3</sub>, NaBr, Na<sub>2</sub>SO<sub>4</sub>, Na<sub>2</sub>CO<sub>3</sub> and NaF were added into the solution. The interference effects of different types and concentrations of anions on the Pb<sup>2+</sup> adsorption capacity of FNMs-Cys were investigated.

### 2.8. Analysis Methods

On the basis of the adsorption experiment, Eqs (1) and (2) were used to calculate the equilibrium adsorption capacity and removal rate [22].

$$q_{e} = \frac{(c_{0} - c_{e}) \times V}{m} \tag{1}$$

$$\eta = \frac{(c_0 - c_e)}{c_0} \times 100 \tag{2}$$

Where  $q_e$  is adsorption capacity (mg/g);  $C_0$  and  $C_e$  (mg/L) are the initial concentration and the instantaneous concentration, respectively. m is the dose of adsorbent (g); V is the volume of solution (L);  $\eta$  Is Pb<sup>2+</sup> removal rate (%).

In addition, according to the adsorption experiment [23], quasi-first-order kinetic model eq (3) and quasi-second-order kinetic model eq (4) were selected to calculate the kinetics:

$$\ln(q_e - q_t) = \ln q_{e,cal} - k_1 \times t \tag{3}$$

$$\frac{t}{q_{t}} = \frac{1}{k_2 \times q_{e,cal}^2} + \frac{t}{q_{e,cal}} \tag{4}$$

Where,  $q_e$  is the equilibrium adsorption capacity (mg/g),  $q_t$  (mg/g) is the adsorption capacity of  $pb^{2+}$  solution at time t (h),  $q_{e,cal}$  (mg/g) is the theoretical maximum adsorption capacity,  $k_1$  (Min-1) and  $k_2$ [g/(mg·min)] are the quasi-first-order rate constant and quasi-second-order rate constant of the kinetic model, respectively.

In order to further study the diffusion mechanism [24], Eq(5)of intra-particle diffusion kinetics was selected to calculate the intra-particle model, and Eq(6)of Elovich model was used to describe the adsorption/desorption kinetics, as shown below:

$$q_{t} = k_{i} \times t^{0.5} + C \tag{5}$$

$$q_t = \frac{\ln(\alpha \times \beta)}{\beta} + \frac{\ln(t)}{\beta} \tag{6}$$

 $k_i$  is the diffusion rate constant within the particle, C (mg/g) is the constant related to the thickness of the surface layer,  $\alpha$  is the Elovich rate constant.  $\beta$  is the change of adsorbent surface coverage.

Langmuir (Eq.(7)), Freundlich (Eq.(8)) and Temkin (Eq.(9)) adsorption isotherm models were used to fit the adsorption of FNMs-Cys, as follows [25]:

Langmuir isothermal model:

$$q_{\rm e} = q_{\rm m} K_{\rm L} c_{\rm e} / (1 + K_{\rm L} c_{\rm e}) \tag{7}$$

Where  $q_m$  (mg/g) is the theoretical maximum adsorption capacity and  $K_L$  (L/mg) is Langmuir isotherm constant.

Freundlich isothermal model:

$$q_e = KFc_e^{1/n} \tag{8}$$

Where KF (L/mg) is Freundlich constant, 1/n is constant of adsorption process, 1/n is isotherm type, 1/n < 0 is irreversible, 0 < 1/n < 1 is ideal, and 1/n > 1 is not ideal.

Temkin isothermal model:

$$q_e = RT(\ln K_T C_e)/b_T \tag{9}$$

Where,  $b_T$  is the constant related to the adsorption heat defined by Temkin, R is the universal gas constant (8.314 J/mol), and T is the Kelvin temperature.

D-R isothermal model [26] can be obtained from Eqs(10),(11) and (12):

$$\varepsilon = RT \ln(1 + 1/c_e) \tag{10}$$

$$\ln q_e = \ln q_m - \beta \varepsilon^2 \tag{11}$$

$$E = 1/\sqrt{2\beta} \tag{12}$$

Where  $\epsilon$  is the Polanyi potential, $\beta$  is the activity coefficient associated with the mean adsorption free energy (mol²/J²),E (kJ/mol) is the free energy of the adsorbent transferred from solution to the surface of the adsorbent,In the adsorption process, 8kJ/mol < E < 16kJ/mol was defined as chemisorption, while the adsorption mechanism when E < 8kJ/mol was defined as physical adsorption, which was determined by the slope of the equation D-R isothermal model.

According to the adsorption experiment, Van 'Hoff equation (Eqs(13),(14)and(15)) was selected to explore the relationship between the chemical equilibrium constant and temperature, and the parameters were calculated as follows [27]:

$$K_{\rm c} = \frac{q_{\rm e}}{c_{\rm e}} \tag{13}$$

$$\Delta G = -RT \ln K_{\rm c} \tag{14}$$

$$\ln K_{\rm c} = -\frac{\Delta H}{RT} + \frac{\Delta S}{R} \tag{15}$$

Where Kc is the thermodynamic equilibrium constant and T is the absolute temperature (K).  $\Delta H$  (kJ/mol) is the enthalpy change,  $\Delta G$  (kJ/mol) is the Gibbs free energy, and  $\Delta S$ (J/mol·K) is the entropy change.

### 3. Results and Discussion

## 3.1. Optimization Results of FNMs-Cys Modification Conditions

**Table 1.** Orthogonal experiment of adsorption of Pb<sup>2+</sup> by FNMs-Cys

Experiment number	A.pH	B.Feed ratio	C.Glutaraldehyde dosage (mL)	D.temperature(°C)	Removal rate (%)
1	7.0	1:0.5	0.5	30	71.94
2	7.0	1:1	1	55	93.30
3	7.0	1:1.5	2	80	79.49
4	8.0	1:0.5	1	80	59.91
5	8.0	1:1	2	30	49.37
6	8.0	1:1.5	0.5	55	58.14
7	9.0	1:0.5	2	55	81.76
8	9.0	1:1	0.5	80	78.92
9	9.0	1:1.5	1	30	71.53
K1	244.73	213.61	209.00	218.32	
K2	167.36	221.59	224.74	233.20	
К3	232.21	209.16	211.16	192.84	
k1	81.58	71.20	69.67	72.77	
k2	55.79	73.86	74.91	77.40	
k3	77.40	69.72	70.39	64.28	
Range R	25.79	4.41	5.24	13.12	
Primary and secondary factors	A>D>C>B				
Optimal scheme	$A_1B_2C_2D_2$				

Magnetic mesoporous silica was grafted with cysteine to increase the functional groups on the surface of microspheres and improve the removal rate of  $Pb^{2+}$ . In order to obtain the best modified composites, a four-factor and three-level orthogonal experimental table was designed in this paper to obtain the following 9 composites and the removal rate of each composite. (Table 1)

#### Table 1 shows that:

As can be seen from Table 1, R is an index to evaluate the influence degree of the four influencing factors. The larger the range of R, the stronger the influencing factors. The results show that  $R_A > R_D > R_C > R_B$ , which shows the adsorption effect of magnetic mesoporous silica modified by cysteine, and the order of each factor is pH > reaction temperature > glutaraldehyde dosage > feed ratio,The optimal experimental scheme is  $A_1B_2C_2D_2$ , and the conditions are pH=7, the feed ratio is 1: 1, the dosage of glutaraldehyde is 1 mL and the temperature is 55 °C.

Therefore, the best scheme for the modification of magnetic mesoporous silica cysteine is as follows: 0.2g magnetic mesoporous silica is added to 50ml buffer solution containing 1ml glutaraldehyde in a water bath at  $55\,^{\circ}$ C, after full reaction, the magnet is separated, 0.2g cysteine and 0.2g sodium borohydride are added and stirred for 6 h. After three times of magnetic washing, FNMs-Cys was obtained.

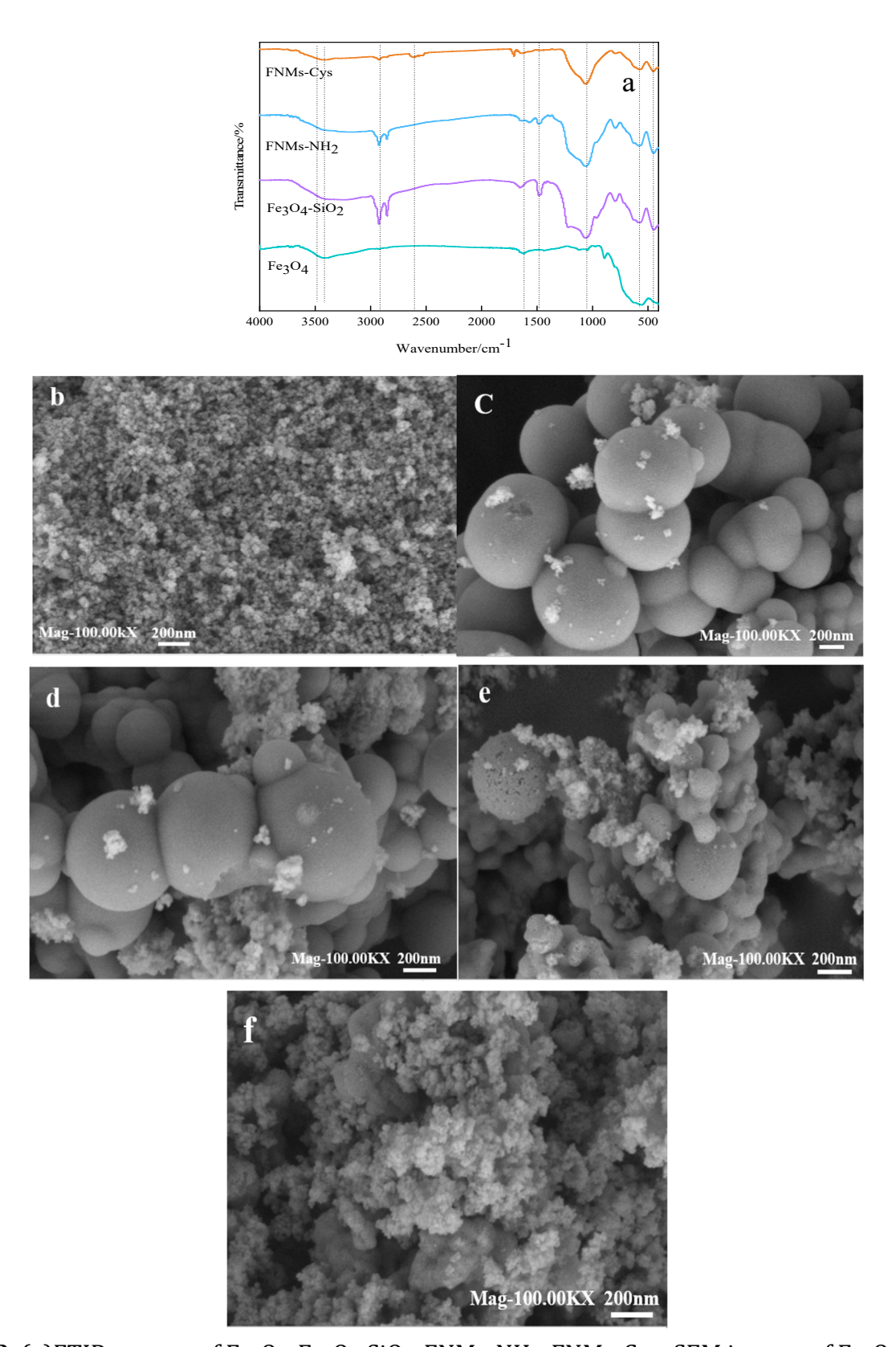
## 3.2. Physical and Chemical Characteristics of FNMs-Cys

FTIR spectra were acquired to determine the differences of functional groups on the surfaces of Fe<sub>3</sub>O<sub>4</sub>, Fe<sub>3</sub>O<sub>4</sub>-SiO<sub>2</sub>, FNMs-NH<sub>2</sub> and FNMs-Cys composites, as well as to assses the changes in the surface functional group structures before and after adsorption were evaluated. The FTIR spectra of the obtained raw materials Fe<sub>3</sub>O<sub>4</sub>, Fe<sub>3</sub>O<sub>4</sub>-SiO<sub>2</sub>, FNMs-NH<sub>2</sub> and FNMs-Cys are shown in the Fig3a. The characteristic absorption peak observed at 597cm<sup>-1</sup> is attributed to the tensile vibration of the Fe-O bond [28]. The strong absorption peak observed at 1057cm<sup>-1</sup> is attributed to the lattice vibration of Si-O-Si and the stretching vibration of Si-O band [29]. The stretching vibration band [30] of C-H is 2930 cm<sup>-1</sup>, The absorption peak observed at 1640cm<sup>-1</sup> is the overlap of the N-H bending vibration peak and the bending vibration band of the O-H absorption peak into a wide absorption band. The peak observed at 2601 cm<sup>-1</sup> is attributed to the grafted cysteine-SH [31] absorption peak, and the free carboxylate O-H [32] stretching vibration absorption is located at 3550 cm<sup>-1</sup>. 1720 cm<sup>-1</sup> is the stretching vibration peak of free carboxylic acid C=O. These data confirmed that SiO<sub>2</sub> was successfully coated on the surface of Fe<sub>3</sub>O<sub>4</sub> nanospheres, and cysteine was successfully grafted onto the surface of magnetic mesoporous silica.

Fig 3(b)-(f)shows the SEM morphologies of Fe<sub>3</sub>O<sub>4</sub>, Fe<sub>3</sub>O<sub>4</sub>-SiO<sub>2</sub>, FNMs-NH<sub>2</sub>, FNMs-Cys and FNMs-Cys-Pb at 10W magnification. Comparing the results of Fe<sub>3</sub>O<sub>4</sub> with Fe<sub>3</sub>O<sub>4</sub>-SiO<sub>2</sub>, FNMs-NH<sub>2</sub> and FNMs-Cys, it can be found that regular magnetic silica microspheres are formed after modification<sup>4</sup>. Because the microspheres are magnetic and attractive to each other, there is a phenomenon of reunion between the microspheres. Nano-particles appear outside the silica microspheres loaded with functional groups, which makes their surfaces rougher, which also provides more attachment sites for adsorption, thus promoting greater adsorption. Careful observation of the 10 W times SEM image of FNMs-Cys shows that the surface of microspheres has irregular pore structure. Comparing FNMs-Cys and FNMs-Cys-Pb before and after adsorption, it can be found [33] that the adsorbed FNMs-Cys-Pb still maintains the shape of microspheres, and the particles on the surface of microspheres increase sharply compared with those before adsorption, indicating that the adsorbent FNMs-Cys has a good adsorption effect on Pb<sup>2+</sup>.

In addition, the EDS mapping of FNMs-Cys and FNMs-Cys-Pb is shown in the Fig 4a from which we can see the distribution and changes of elements of C, N, Si, O, Fe and Pb, which can more intuitively show whether FNMs-Cys has adsorbed Pb<sup>2+</sup>. As can be seen from the Fig 4b, the

representative color of  $Pb^{2+}$  in the adsorbed FNMs-Cys-Pb begins to appear, and from the distribution of  $Pb^{2+}$ , the adsorbed  $Pb^{2+}$  is in a state of uniform distribution [34], which further shows that FNMs-Cys has a good adsorption effect on  $Pb^{2+}$  in the solution.



 $\label{eq:Fig3} \textbf{Fig 3.} \ (a) FTIR\ spectra\ of\ Fe_3O_4, Fe_3O_4-SiO_2, FNMs-NH_2, FNMs-Cys; SEM\ images\ of\ Fe_3O_4\ (b), Fe_3O_4-SiO_2\ (c), FNMs-NH_2\ (d), FNMs-Cys\ (e), and\ FNMs-Cys-Pb\ (f);$ 

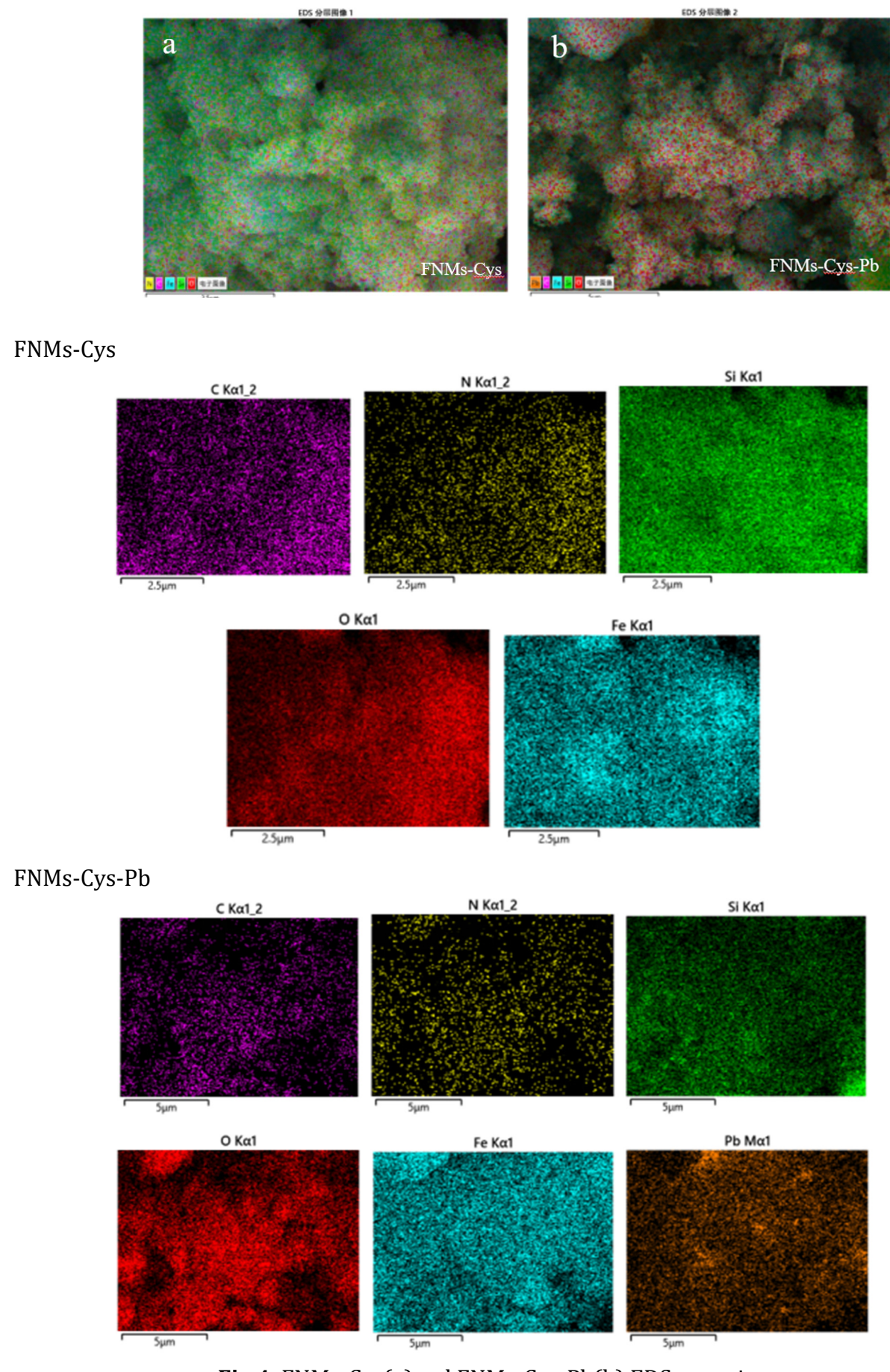


Fig 4. FNMs-Cys(a)and FNMs-Cys-Pb(b) EDS-mapping

The crystalline structure of FNMs-Cys was characterized by XRD analysis, and the chemical compositions of Fe<sub>3</sub>O<sub>4</sub>, Fe<sub>3</sub>O<sub>4</sub>-SiO<sub>2</sub>, FNMs-NH<sub>2</sub>, FNMs-Cys and FNMs-Cys-Pb were tested respectively, and the results are shown in the Fig 5(c).Fe<sub>3</sub>O<sub>4</sub>-SiO<sub>2</sub>,FNMs-NH<sub>2</sub>, FNMs-Cys and FNMs-Cys-Pb all have characteristic diffraction peaks at 30.1°, 35.4°, 43.1°, 53.4°, 56.9° and 62.5°. Corresponding to pure Fe<sub>3</sub>O<sub>4</sub> crystal faces (220), (311), (400), (422), (511) and (440). By comparing the characteristic peaks of FNMs-Cys and FNMs-Cys-Pb, the peak of Fe<sub>3</sub>O<sub>4</sub> decreases, which is consistent with the report [34-36]. the peak area is smaller than the characteristic diffraction peaks of Fe<sub>3</sub>O<sub>4</sub>, Fe<sub>3</sub>O<sub>4</sub>-SiO<sub>2</sub>, FNMs-NH<sub>2</sub> and FNMs-Cys.The results showed [37] that the adsorption of Pb<sup>2+</sup> by FNMs-Cys increased the disorder degree of Fe<sub>3</sub>O<sub>4</sub>, and the addition of Pb<sup>2+</sup> reduced the ordering of the composites.

In order to better study the specific surface area of modified FNMs-Cys, BET method was used to analyze the structural characteristics of the samples. The BET results of  $Fe_3O_4$ ,  $Fe_3O_4$ -SiO<sub>2</sub> and FNMs-Cys are shown in the Fig 5(a)(b) and table 2. According to IUPAC classification, the adsorption-desorption isotherms of  $Fe_3O_4$ -SiO<sub>2</sub> and FNMs-Cys are both type IV [38], with adsorption hysteresis loops, indicating that the porous adsorbent has a capillary condensation system, and the mesoporous structure is dominant in the material. It can be seen from Table 2 that  $Fe_3O_4$ -SiO<sub>2</sub> is a mesoporous composite with a small pore volume of 0.10 cm<sup>3</sup>/g, a medium pore size of 15.44 nm and a medium specific surface area of 30.07 m<sup>2</sup>/g; After amino acid modification, FNMs-Cys also has mesopores (9.12 nm) between 2 nm and 50 nm. Because of cysteine loading, although the average pore size decreased slightly [39], the grafted cysteine increased the specific surface area of FNMs-Cys (42.97 m<sup>2</sup>/g).

TG can usually be used to evaluate the thermal stability of materials and the proportion of each component.  $N_2$  protection was selected to prevent  $Fe_3O_4$  oxidation from affecting the experimental results. The heat loss of  $Fe_3O_4$ ,  $Fe_3O_4$ -SiO<sub>2</sub> and FNMs-Cys was tested at  $40 \sim 800\,^{\circ}\text{C}$  with the TG curve at the heating rate of  $10\,^{\circ}\text{C}$ /min as shown in Fig 5(d). When it was close to  $800\,^{\circ}\text{C}$ , the weight loss rates of  $Fe_3O_4$ ,  $Fe_3O_4$ -SiO<sub>2</sub> and FNMs-Cys were respectively The weight loss of FNMs-Cys can be roughly divided into three stages. In the first stage, the weight loss rate of FNMs-Cys is 4.56% at  $0 \sim 145\,^{\circ}\text{C}$ , which corresponds to the water molecules existing in FNMs-Cys and the evaporation of water molecules [40], which also proves that FNMs-Cys is hydrophilic. In the second stage, the temperature dropped rapidly from 145 to  $270\,^{\circ}\text{C}$ , and the weight loss rate of FNMs-Cys was 19.07%. Because the boiling point of silane coupling agent was  $217\,^{\circ}\text{C}$ , APTES and cysteine grafted on the surface of FNMs-Cys were decomposed by heat [41]. In the third stage, the weight loss rate of FNMs-Cys was 28.08% when it decreased slowly from  $279\,^{\circ}\text{C}$  to  $567\,^{\circ}\text{C}$ , which mainly corresponded to the dehydration and condensation of silicon hydroxyl groups on the surface of silica microspheres, and was similar to the curve of  $Fe_3O_4$ -SiO<sub>2</sub>.

Experimental results of saturation strength and hysteresis curves of VSM magnetic field of Fe<sub>3</sub>O<sub>4</sub>, FNMs-Cys, and FNms-Cys-Pb at room temperature are shown in the Fig 5(e). Fe<sub>3</sub>O<sub>4</sub>, FNMs-Cys and FNms-Cys-Pb all have superparamagnetism, and the magnetic properties of the three materials are 68.8emu/g, 58.4emu/g, respectively. The hysteresis curves are all shaped as "S", and the three curves all pass through the origin, indicating that the coercive force is approximately zero [42]. The magnetic properties of the modified FNMs-Cys were slightly lower than that of Fe<sub>3</sub>O<sub>4</sub> (5.0 emu/g), indicating that the modified FNMs-Cys still maintained excellent magnetic separation performance. The reason for the decrease in magnetic properties was that the coating of silica and the load of functional groups would both lead to the decrease in magnetic properties of the materials. After Pb<sup>2+</sup> adsorption, the magnetic properties of FNMs-Cys-Pb decreased only 5.4 emu/g, still maintaining good magnetic separation performance. By comparing the dispersion properties of Fe<sub>3</sub>O<sub>4</sub>, FNMs-Cys, and FNms-Cys-Pb in aqueous solution, it can be intuitively seen from the figure that all three have good dispersion, but FNMs-Cys and

FNms-Cys-Pb have better dispersion than  $Fe_3O_4$ . The figure shows the magnetic separation performance of FNMs-Cys and FNMs-Cys-Pb. It can also be intuitively seen from the Fig 5(f)that under the action of external magnetic field, both of them can be quickly separated within 3 min, thus realizing rapid recovery and reuse in the actual treatment process.

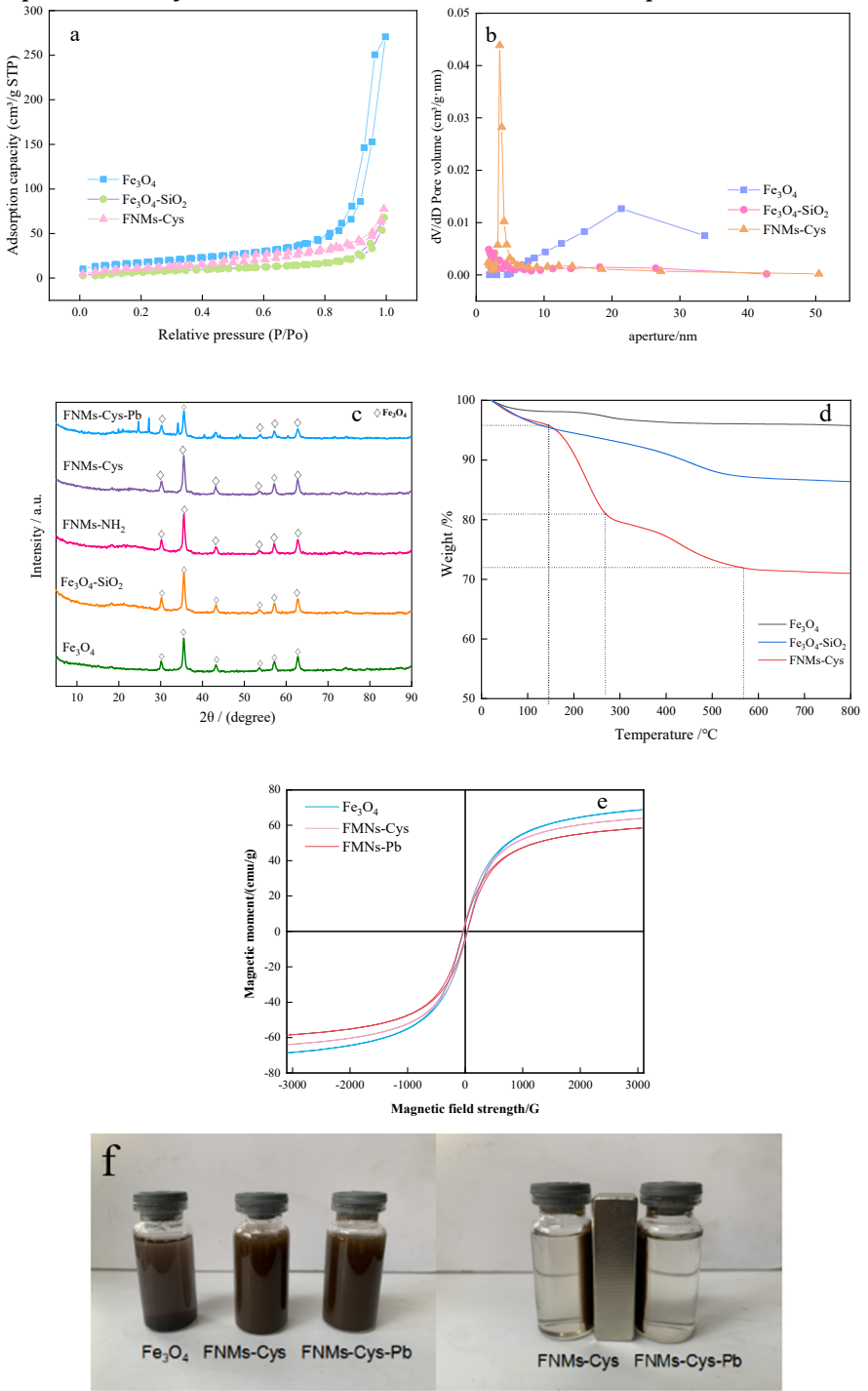


**Fig 5.** (a,b)BET spectra of Fe<sub>3</sub>O<sub>4</sub>, Fe<sub>3</sub>O<sub>4</sub>-SiO<sub>2</sub> and FNMs-Cys; (c)XRD patterns of Fe<sub>3</sub>O<sub>4</sub>, Fe<sub>3</sub>O<sub>4</sub>-SiO<sub>2</sub>, FNMs-NH<sub>2</sub>, and FNMs-Cys and FNMs-Cys-Pb;(d)TG spectra of Fe<sub>3</sub>O<sub>4</sub>, Fe<sub>3</sub>O<sub>4</sub>-SiO<sub>2</sub> and FNMs-Cys; (e)Hysteresis curves of Fe<sub>3</sub>O<sub>4</sub>, Fe<sub>3</sub>O<sub>4</sub>-SiO<sub>2</sub> and FNMs-Cys-Pb; (f)Comparison of dispersion performance and magnetic separation performance of Fe<sub>3</sub>O<sub>4</sub>, FFNMs-Cys , and FNMs-Cys-Pb

**Table 2.** Pore volume, pore size, and specific surface area of Fe<sub>3</sub>O<sub>4</sub>, Fe<sub>3</sub>O<sub>4</sub>-SiO<sub>2</sub> and FNMs-Cys

	Pore volume (cm <sup>3</sup> /g)	Average of pore width (nm)	BET surface (m <sup>2</sup> /g)
Fe <sub>3</sub> O <sub>4</sub>	-	-	67.71
Fe <sub>3</sub> O <sub>4</sub> -SiO <sub>2</sub>	0.10	15.44	30.07
FNMs-Cys	0.12	9.12	42.97

# 3.3. Influence of Various Operation Conditions on Batch Adsorption Properties3.3.1. Effect of Adsorption Materials

Based on the optimization results of modification conditions of adsorption materials, the adsorption effects of Fe<sub>3</sub>O<sub>4</sub>-SiO<sub>2</sub>, FNMs-NH<sub>2</sub> and FNMs-Cys on Pb<sup>2+</sup> were explored. Under the same conditions, the adsorption capacity of Fe<sub>3</sub>O<sub>4</sub>-SiO<sub>2</sub>, FNMs-NH<sub>2</sub> and FNMs-Cys is 67.55mg/L, 98.65mg/L and 168.77mg/L respectively. As can be seen from the Fig 6(a), the adsorption effect of FNMs-Cys on Pb<sup>2+</sup> is much greater than that of Fe<sub>3</sub>O<sub>4</sub>-SiO<sub>2</sub> and FNMs-NH<sub>2</sub>, which shows that the modification experiment can increase the adsorption effect of adsorption .

## 3.3.2. Effect of pH

The effect of the solution pH can be associated with a number of mechanisms such as metal speciation in solution, change of the ionic forms of the functional groups on the silica surface, and the competition effects of proton ions with metal ions [43]. Fig 6(b) shows the effect of the pH on the removal of Pb<sup>2+</sup> metal ions as the function of the solution pH in the range of 1-7.As shown in the Figure, in the range of 1 to 7, the absorption of Pb<sup>2+</sup> increases with the increase of PH from 1 to 6, and the adsorption capacity increases from 51.47 mg/g to 174.85 mg/g. At this time, the adsorption of Pb<sup>2+</sup> by FNMs-Cys reaches the maximum value, while the adsorption of Pb<sup>2+</sup> decreases when pH is greater than 6.Therefore, the increase in the metal removal with increasing pH can be explained on the basis of a decrease in competition between proton ions (H + ) and positively charged metal ions at the adsorbent surface sites, The concentration of H+ in the solution gradually decreases, and the adsorbent can provide enough adsorption sites to adsorb Pb<sup>2+</sup>. It is also important to note that at the pH more than 6, the precipitation of metal cations in basic medium occurs because of the forming of metals hydroxides which can be reduced the adsorption efficiency. To explain this observation, the presence of the main metal ion  $M^{2+}$  species is M (OH) <sub>2</sub> at pH > 6, and at pH < 6 is  $M^{2+}$  and M (OH) +. therefore, most ions are not accessible to adsorb at higher pH values and consequently the removal efficiency is decreased. Therefore, in this study, pH=6 was chosen as the optimum pH for all following experiments.

#### 3.3.3. Effect of Adsorbent Dosage

In order to study the removal efficiency of  $Pb^{2+}$ , the effect of adsorbent dose was studied. As can be seen from the Fig 6(c), when the initial pH is 6, the effects of different FNMs-Cys additions (0~50mg) on the adsorption capacity and removal rate of 100 mg/L  $Pb^{2+}$ . The results showed that the removal of  $Pb^{2+}$  increased from 61.34% to 99.74% for  $Pb^{2+}$ .

The adsorption of metal ions increases with the increase of adsorbent dosage, which means that the active sites on the adsorbent surface increase and more connecting sites are formed. When the amount of adsorbent increases, the removal rate of  $Pb^{2+}$  increases, When the amount of FNMs-Cys adsorbent continues to increase to 50 mg, the adsorption was 171.62 mg/g, and the adsorption reaches equilibrium, at which time the removal rate is 99.74%. Therefore, 50 mg of adsorbent was used in subsequent experiments.

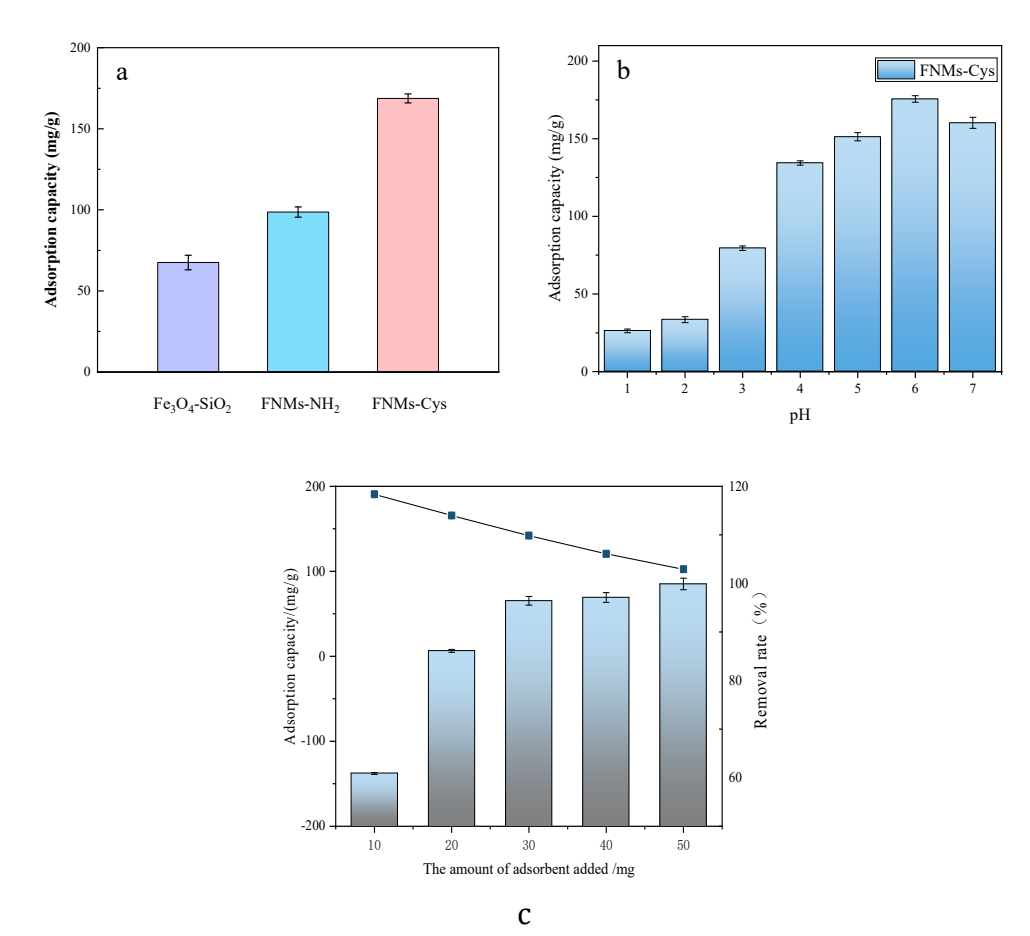


**Fig 6.** Influence of (a) Different Amino Acid Modified Materials;(b) pH and (c) Dosage of adsorbent on the removal of lead and cobalt using FNMs-Cys

Maximum adsorption capacity

**Table 3.** Comparison of Pb<sup>2+</sup> removal rates of other materials

number	absorbent material	maximum adsorption capacity	removal rate	references
1	Natural zeolite	66mg/L	28.84%	7
2	Chitosan/polyvinyl alcohol blends	7.67 mg/L	94%	9
3	MnO <sub>2</sub> /CS	126.1 mg/L	83.7%	44
4	$Fe_3O_4$ - $MnO_2$ - $SiO_2$ - $NH_2$	100mg/L	93.66%	15
5	Cys-Fe <sub>3</sub> O <sub>4</sub> MNPs	183.5mg/L	84.18%%	18
6	MSCMNPs-S system	170.27mg/L	95.7%	16
7	FNMs-Cys	178.57 mg/g	99.76%	this study

It is obvious that the magnetic nanoparticles have a stronger adsorption capacity and a higher efficiency in removing lead ions than materials such as natural zeolites, although it is prone to oxidation and aggregation, fortunately, coating  $Fe_3O_4$  particles with a  $SiO_2$  layer by silylation prevents the oxidation and aggregation of  $Fe_3O_4$ , and also improves its chemical stability. Fan et al [45]. used  $SiO_2$  as a core-shell for the modification of the magnetic silica nanoparticles which has good selectivity for the extraction of toxic metal ions from aqueous media, in addition specific organic or inorganic compounds for surface modification can improve the adsorption efficiency of these nanoparticles, Vojoudi et al [16]. used bis(3-triethoxysilylpropyl)

tetrasulphide (MSCMNPs-S4) for further modification of magnetic nanomaterials, and under the optimized conditions, the nanosorbents showed an adsorption capacity of up to 270.27 mg/L, which improved the lead removal rate. However, the removal efficiency was still lower than 99.76% used in this paper.

The reason may be that after the surface modification of cysteine, its -SH,-NH<sub>2</sub>,-COOH functional groups provide good biocompatibility and stability, and through the formation of a variety of complexes and thus well involved in the removal of metal ions from the aqueous solution, the porous structure also provides more sites for the adsorption of lead.

## 3.4. Adsorption Kinetics

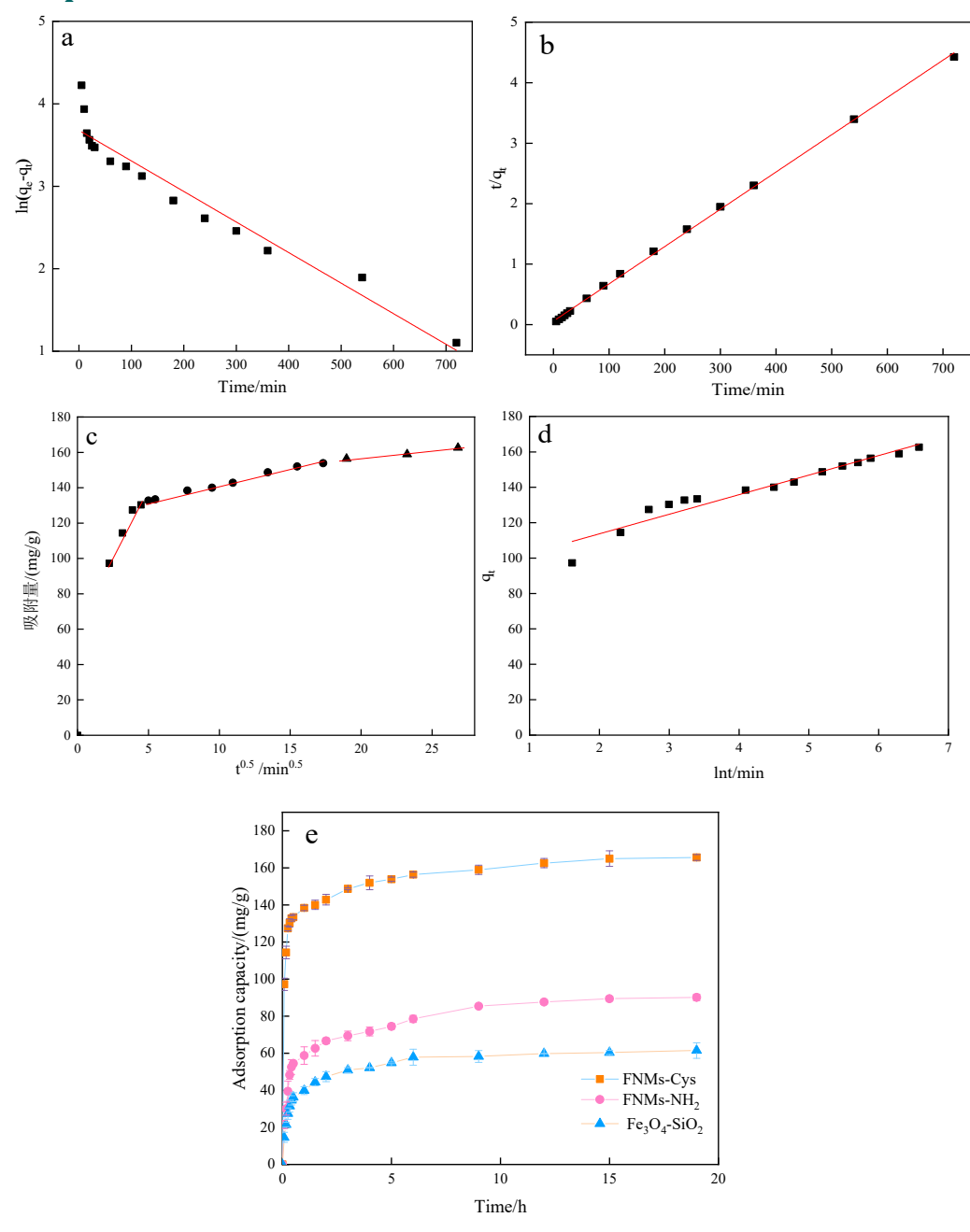


**Fig 7.** quasi-first-order kinetic model (a), quasi-second-order kinetic model (b), In-particle diffusion model (c), Elovich model (d) and Influence of adsorption time on adsorption effect(e)

As shown in the Fig 7(e), the effects of  $Fe_3O_4$ -SiO<sub>2</sub>, FNMs-NH<sub>2</sub> and FNMs-Cys on the adsorption capacity of 100 mg/L Pb<sup>2+</sup> at different adsorption times were determined. The results showed that the adsorption processes of  $Fe_3O_4$ -SiO<sub>2</sub>, FNMs-NH<sub>2</sub> and FNMs-Cys almost reached equilibrium within 4 hours, and the adsorption capacity of FNMs-Cys was higher than that of  $Fe_3O_4$ -SiO<sub>2</sub> and FNMs-NH<sub>2</sub>. Adsorption kinetic model is widely used to analyze the dynamic adsorption behavior in batch system and reveal the mass transfer mechanism, which is convenient for understanding the adsorption performance and process of Pb<sup>2+</sup> by FNMs-Cys . Therefore, the quasi-first-order kinetic model, quasi-second-order kinetic model, Elovich model and intra-particle diffusion kinetic model were selected to fit the Pb<sup>2+</sup> adsorption capacity of FNMs-Cys in different time ranges [46]. Fig 7 (a)-(e)and Table 4 summarize the quasi-first-order kinetic model, quasi-second-order kinetic model and intra-particle diffusion kinetic model, as well as the corresponding parameters and data.

Compared the R<sup>2</sup> of the quasi-first-order kinetic model and the quasi-second-order kinetic model, the correlation coefficient (R<sup>2</sup>=0.999) obtained by the quasi-second-order kinetic model shows a higher fitting degree with the experimental data, while the R<sup>2</sup> of the quasi-first-order kinetic model is only 0.931. The assumption of pseudo-second-order kinetics is that the reaction process is based on chemical adsorption, that is, the chain force or ion/electron exchange combination between metal ions and adsorption materials, so the adsorption rate of FNMs-Cys is controlled by chemical adsorption. The main migration state of Pb<sup>2+</sup>in the adsorption process and the adsorption process in each stage can be judged by the intra-particle diffusion kinetic model. Almost all adsorption sites of FNMs-Cys exist on its surface, so adsorbents can easily enter these active sites, so in the initial stage. The slopes of the three stages gradually decrease, indicating that the adsorption rate gradually decreases, and it is in a slow diffusion stage, and Pb<sup>2+</sup> continuously diffuses to micropores, and finally reaches the adsorption equilibrium. The multi-stage adsorption process shows that this reaction is not limited to the influence of diffusion factors, but also has other effects. Elovich model is a dynamic model to explore the adsorption capacity on the basis of chemical adsorption, and R<sup>2</sup>=0.930 once again proves that the adsorption process is chemical adsorption [45, 47].

**Table 4.** Fitting parameters of FNMs-Cys adsorption kinetics model for Pb<sup>2+</sup>

model		parameter	FNMs-Cys
		$R^2$	0.931
Quasi-first-order kinet	k <sub>1</sub> (min <sup>-1</sup> )	0.003	
<b>L</b>		$q_{e,cal}$ (mg/g)	39.581
		$R^2$	0.999
Quasi-second-order kinetic model		$k_2$ (g/(mg·min))	6.613×10 <sup>-4</sup>
		$q_{e,cal}$ (mg/g)	162.074
		α	4.399×10 <sup>4</sup>
Elovich model		β	0.090
		$R^2$	0.930
	0-20 min	$R^2$	29.888
		$k_1$ (min <sup>-1</sup> )	11.727
		$q_{e,cal}$ (mg/g)	0.911
	25-300 min	$R^2$	1.776
Intra particle diffusion model		$k_2$ (g/(mg·min))	123.920
•		$q_{e,cal}$ (mg/g)	0.991
	360-900 min	α	0.782
		β	141.335
		$R^2$	0.930

## 3.5. Adsorption Isotherm

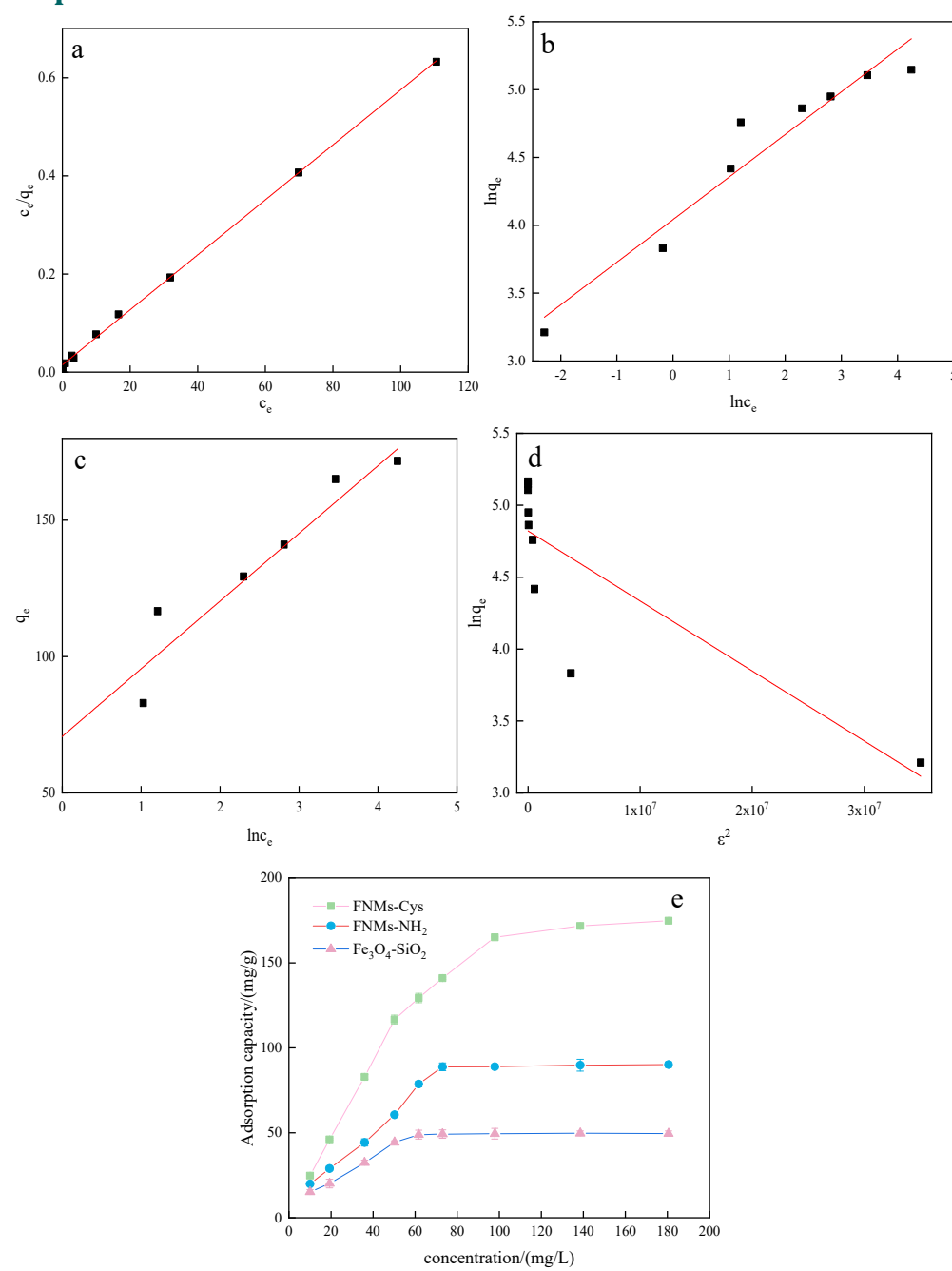


**Fig 8.** Langmuir model (a), Freundlich model (b), Temkin model (c), D-R model (d) and Influence of initial concentration on adsorption effect(e)

As shown in the Fig 8(e), the influence of the change of  $Pb^{2+}$  solution concentration on  $Pb^{2+}$  adsorption capacity of  $Fe_3O_4$ -SiO<sub>2</sub>, FNMs-NH<sub>2</sub> and FNMs-Cys in the same adsorption time was determined. The experimental results show that the adsorption capacity of FNMs-Cys is always higher than  $Fe_3O_4$ -SiO<sub>2</sub> and FNMs-NH<sub>2</sub>, and the composite material FNMs-Cys modified by magnetic mesoporous silica obviously improves  $Pb^{2+}$ , and the adsorption capacities of the three materials also increase with the increase of solution concentration. When the solution concentration reached 100 mg/L, the concentration increased again, and the adsorption capacity of  $Pb^{2+}$  by FNMs-Cys increased slowly. In addition, in order to further explore the capacity of the adsorbent itself, three adsorption isotherm models, Langmuir, Freundlich and Temkin, were used to fit and analyze the adsorption behavior of FNMs-Cys. Fig 8(a)-(d)and

Table 5 summarize the corresponding parameters and data. From the experimental data, it can be concluded that the adsorption of  $Pb^{2+}$  by FNMs-Cys is more in line with Langmuir adsorption isotherm model ( $R^2$ =0.999), indicating that the adsorption process of  $Pb^{2+}$  by FNMs-Cys is monolayer adsorption [48]. According to Langmui model, when the solution concentration is 180 mg/L, the theoretical maximum adsorption capacity qm of FNMs-Cys reaches 178.57 mg/g, which is close to the actual adsorption capacity (174.85 mg/g). In addition, when the 1/n in Freundlich model is between 0 and 1, it is more beneficial to the adsorption process. In this study, the 1/n of FNMs-Cys is 0.313, which indicates that the adsorption process is forward, and it shows that the adsorption process is chemical monolayer adsorption [49]. However, the fitting  $R^2$  of D-R isothermal model is 0.648, which does not have good fitting. [50]

model	parameter	FNMs-Cys
	$R^2$	0.999
Langmuir model	$q_m  (\text{mg/g})$	178.57
	$K_L(L/mg)$	0.379
	$R^2$	0.923
Freundlich model	$K_F(L/mg)$	56.949
	1/n	0.313
	В	24.833
Tomkin model	$lpha_{ m T}$	17.222
Temkin model	$b_{\mathrm{T}}$	133.248
	$R^2$	0.939
	$q_m (mg/g)$	124.109
D-R model	β	4.865
	$R^2$	0.648

**Table 5.** Fitting parameters of FNMs-Cys adsorption isothermal model for Pb<sup>2+</sup>

#### 3.6. Thermodynamic Analysis

As can be seen from Fig 9(a), when the temperature is  $10^{\circ}$ C, the adsorption capacity of FNMs-Cys on 100 mg/L Pb<sup>2+</sup> is 75.75 mg/g, and the adsorption capacity increases with the increase of temperature. When the temperature rose to 20°C, the adsorption capacity of FNMs-Cys on Pb<sup>2+</sup> reached 121.15 mg/g. When the temperature was 33 ℃, the adsorption capacity increased to 175.82 mg/g. When the temperature reaches the maximum 55°C, the adsorption capacity also reaches the maximum 181.55 mg/g. The slope of the adsorption curve gradually decreases. After 33 °C, the adsorption capacity increases slowly. In order to further understand the adsorption mechanism of FNMs-Cys on Pb2+, Van 'thoff equation was fitted, and thermodynamic parameters(Fig 9b) and relevant data were obtained (Table 6).ΔS is greater than 0, indicating that with the increase of temperature, the randomness of the interface between adsorbent and adsorbed object increases. This randomness is mainly due to the complexation of Pb<sup>2+</sup> with amino and carboxyl functional groups, which increases the mobility and deionization rate of proton from the surface. [51]  $\Delta H=37.802$  kJ/mol adsorption enthalpy change is in the category of chemisorption, which is attributed to chemisorption. The temperature is inversely proportional to  $\Delta G$ , and  $\Delta G$  is less than 0, indicating that the process is spontaneous adsorption at room temperature. It can also be seen from the thermodynamic parameters that the adsorption of pb<sup>2+</sup> by FNMs-Cys is an endothermic process, and the increase of temperature is conducive to adsorption. [52-53]

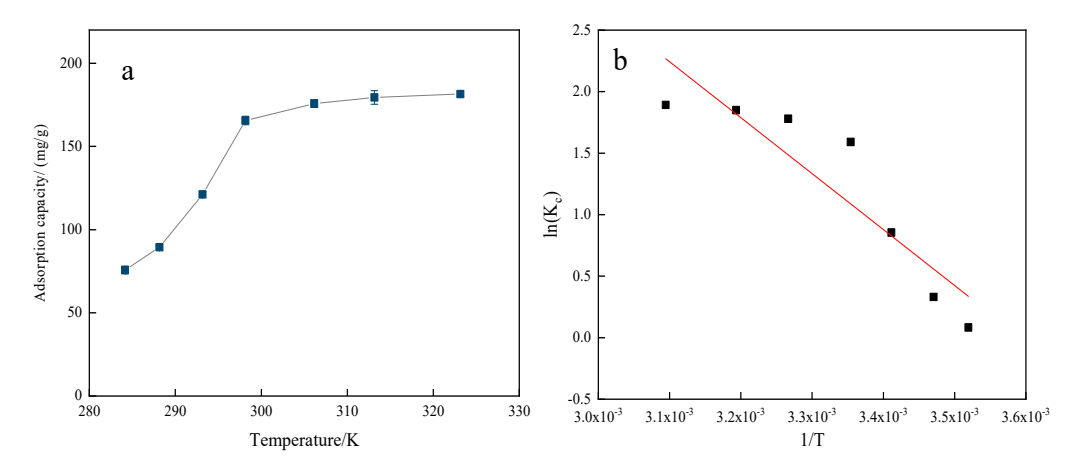


**Fig 9.** Influence of temperature on adsorption effect (a) and thermodynamic analysis of Pb<sup>2+</sup> adsorption by FNMs-Cys (b)

<i>T</i> (K)	$\Delta G(kJ/mol)$	ΔH(kJ/mol)	∆S(J/mol·K)
284.15	-0.20		
288.15	-0.79		
293.15	-2.08		
300.15	-3.94	37.802	135.831
306.15	-4.53		
313.15	-4.82		
222.15	E 00		

**Table 6.** Adsorption thermodynamic fitting parameters of Pb<sup>2+</sup> by FNMs-Cys

## 3.7. Anti-interference Evaluation of FNMs-Cys

In the lead-containing wastewater in real life, Pb2+ does not exist alone, and there are many cations and anions coexisting. [53] In this part, by adding the nitrates of Na<sup>+</sup>, K<sup>+</sup>, Ca<sup>2+</sup> and Mg<sup>2+</sup> with the same concentration gradient to form a binary system with Pb<sup>2+</sup>, the interference ability of Na+, K+, Ca<sup>2+</sup> and Mg<sup>2+</sup> on the adsorption of Pb<sup>2+</sup> by FNMs-Cys was explored. As can be seen from Fig 10(a), all cations have different degrees of interference ability to Pb<sup>2+</sup> adsorption of FNMs-Cys, and the interference degree is Ca<sup>2+</sup>>Mg<sup>2+</sup>>Na<sup>+</sup>>K<sup>+</sup>. The magnitude of the ionic charge determines the magnitude of the interference effect, the smaller the ionic charge, the smaller the interference on FNMs-Cys, which hardly constitutes a competitive adsorption, Na<sup>+</sup> and K<sup>+</sup> have little effect on the Pb<sup>2+</sup> adsorption capacity of FNMs-Cys, and from the point of view of electrostatic attraction, the ionic charges of Na<sup>+</sup> and K<sup>+</sup> are smaller than those of Pb<sup>2+</sup>, Ca<sup>2+</sup>, and Mg<sup>2+</sup>, and therefore are not easily adsorbed by functional groups such as amino and carboxyl groups on FNMs-Cvs. Therefore, it can also be judged that the electrostatic adsorption effect is not the most important adsorption mechanism for the adsorption of Pb<sup>2+</sup> by FNMs-Cys. The concentration of coexisting ions was negatively correlated with the adsorption capacity. When the concentration of coexisting ions increased to 0.1 mol/L, the adsorption capacity of FNMs-Cys on 100 mg/L Pb<sup>2+</sup> decreased from 170.62 mg/g to 142.38 mg/g, 139.55 mg/g, 121.29 mg/g, and 108.76 mg/g, respectively, and the adsorption capacity of FNMs-Cys on Pb2+ decreased from 170.62 mg/g to 142.38 mg/g, 139.55 mg/g, 121.29 mg/g and 108.76 mg/g, respectively. Cys adsorption capacity of P<sup>2+</sup> continued to decrease when the concentration of coexisting ions increased to 0.2 mol/L.

In addition, the interference effects of different types of anions and concentrations on the  $Pb^{2+}$  adsorption capacity of FNMs-Cys were also explored. Six representative anions were selected, namely  $Cl^{-}$ ,  $NO_{3}^{-}$ ,  $Br^{-}$ ,  $SO_{4}^{2-}$ ,  $CO_{3}^{2-}$  and  $F^{-}$ . From Fig 10(b), it can be seen that the six anions have little interference with the  $Pb^{2+}$  adsorption capacity of FNMs-Cys  $^{55}$ ., and the one with the least

influence is Br<sup>-</sup>. whose adsorption capacity for Pb<sup>2+</sup> is 167.25 mg/g, which is only slightly lower than that in the absence of anions (169.62 mg/g).  $NO_3$ - had the greatest interference effect, and the adsorption capacity of FNMs-Cys on Pb<sup>2+</sup> was 147.84 mg/g. Because the presence of nitrate causes an ion exchange process with lead ions, lead nitrate (Pb( $NO_3$ )<sub>2</sub>) is generated through competitive adsorption and reaction, and the solution pH is adjusted so as to reduce the adsorption of lead ions.

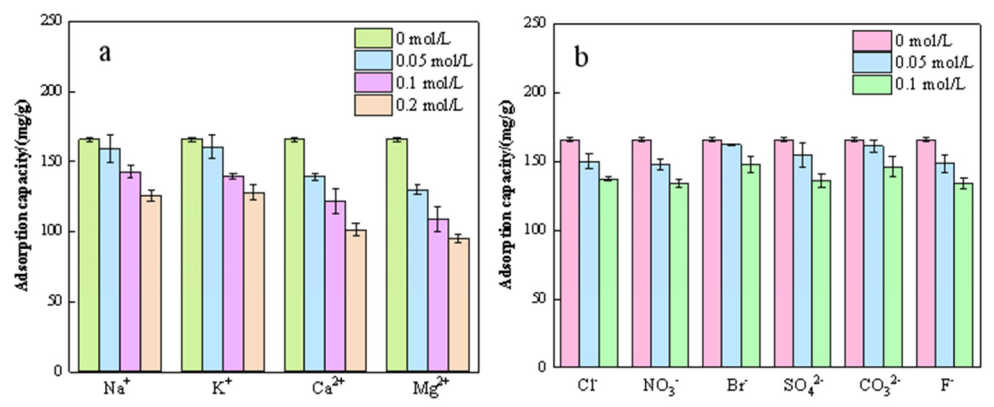


**Fig 10.** Influence of different interfering cations(a) and different interfering anions(b)on the adsorption capacity of Pb<sup>2+</sup> by FNMs-Cys

## 3.8. Reproducibility of FNMs-Cys

In order to verify the reproducibility of FNMs-Cys and the possibility of recycling, adsorption-desorption experiments were carried out. Generally, strong acids such as hydrochloric acid can regenerate amino and carboxyl functionalized adsorbents after adsorption. It is important to judge whether FNMs-Cys can exist stably in strong acid medium. Therefore, 5 concentration gradient HCl washing solutions were set. It can be seen from the Fig11(a) that the regeneration performance of FNMs-Cys is better with the increase of HCl solution concentration in the range of  $0.01 \sim 0.1$  mol/L. When the HCl solution is 0.1 mol/L, it is more suitable as the regeneration medium, and the Fe<sub>3</sub>O<sub>4</sub> core is stable during the regeneration process.

At the same time, concerned whether the washing time of FNMs-Cys in HCl solution will affect the desorption degree of FNMs-Cys. It was found Fig 11(b) that the longer the washing time, the better the regeneration of the desorbed and reabsorbed FNMs-Cys. When the washing time was 60 min, the adsorption capacity of FNMs-Cys for Pb $^{2+}$  reached 159.23 mg/g. Using 0.1 mol/L HCl solution as washing solution, the washing time was controlled at 60 min, and the Pb $^{2+}$ adsorbed FNMs-Cys(FNMs-Cys-Pb) composite was adsorbed and desorbed. Adsorption-desorption of FNMs-Cys (FNMs-Cys-Pb) composites after adsorption of Pb $^{2+}$  was performed five times . According to the results of the Fig11(c), The removal of Pb $^{2+}$  by FNMs-Cys after five adsorption-desorption cycles was only 14.7% lower than the first time. The adsorption capacity of 139.25 mg/g could still be maintained, indicating that FNMs-Cys had excellent reusability and regeneration. Fig11(d) shows the diagram of recycling process.

Because FNMs-Cys showed a high ability to remove Pb<sup>2+</sup>, understanding the internal mechanism of adsorption materials in heavy metal reaction is helpful for its further application in water pollution control, so the adsorption mechanism of FNMs-Cys in heavy metal adsorption is studied and discussed.

As concluded above, the experimental data of adsorption kinetics show that the adsorption of  $Pb^{2+}$  by FNMs-Cys is more in line with the quasi-secondary kinetic model ( $R^2$ =0.998), and the theoretical adsorption capacity of the quasi-secondary kinetic model (qe,cal of 174.85 mg/g) is also closer to the adsorption capacity at the actual equilibrium (178.57 mg/g), which belongs to chemisorption. The mechanism of the adsorption reaction can be deduced from the

magnitude of E. At E values between 8 and  $16\,\mathrm{kJ/mol}$ , chemical ion exchange is the main process of adsorption.

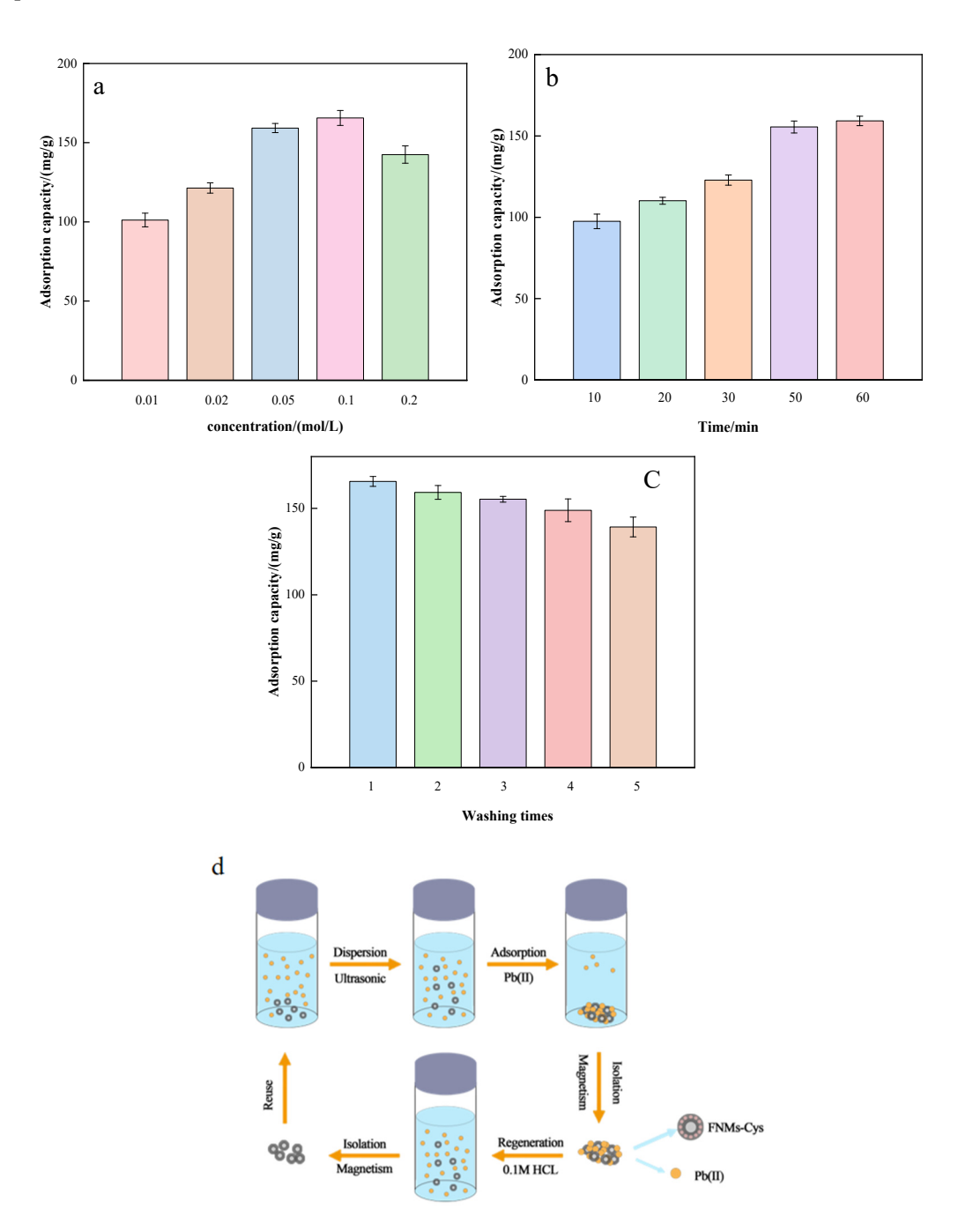


**Fig 11.** Effect of hydrochloric acid concentration (a) washing times (b) on regeneration performance (c) washing time (d)diagram of recycling process

When the E value is higher than 16 kJ/mol, chemical adsorption becomes the main form of adsorption, and the role of ion exchange is minimal. At E values below 8 kJ/mol, adsorption is mainly influenced by physical forces. In the present study, the E-value of the sample was 15.1. The Van'thoff equation was fitted and thermodynamic parameters and correlation data were obtained.  $\Delta S$  is greater than 0, indicating that the stoichiometry between the adsorbent and adsorbate interfaces increases with increasing temperature, and that this stoichiometry is mainly due to an increase in proton mobility and dissociation from the surface due to the complexation of Pb<sup>2+</sup> with amino- and carboxyl-functional groups.  $\Delta H$ = 37.802 kJ/mol enthalpy

change of adsorption is within the realm of chemisorption and also indicates a predominantly chemisorption [54]. which also proves that the adsorption was carried out by chemical ion exchange mechanism.Na+, K+, Ca²+, Mg²+ and different anion concentrations were added to FNMs-Cys adsorption target metal solution (solution containing Pb²+) to judge the influence on adsorption. the existence of coexisting ions has a negative correlation with the binding of FNMs-Cys and Pb²+. Low concentration (0.05 M) of Na+, K+, Ca²+ and Mg²+ has little negative effect on the adsorption of Pb²+ in FNMs-Cys,. The intense competition between high concentration ion coexisting cation solution and target metal solution Pb²+ indicates that cation exchange is involved in the adsorption process. This competitive behavior is not obvious when low concentration cations participate, which indicates that ion exchange is not the decisive factor affecting adsorption [55]. After modification, the surface of FNMs-Cys was detected by FTIR to have a variety of functional groups, including ungrafted amino and hydroxyl groups, as well as grafted carboxyl, amino, and sulfhydryl groups, which were complexed to lead to form strong chemical bonds and surface complexes, such as lead sulfide and lead-carboxylic acid complexes, to remove lead from solution.

## 3.9. Adsorption Mechanism of FNMs-Cys

In addition, from the study of pH value,it can be seen that when the pH is low, the H+ on the surface of the adsorbent forms a competitive adsorption with Pb<sup>2+</sup>, so the adsorption capacity of Pb<sup>2+</sup> is low, and the uptake of Pb<sup>2+</sup> increases when the pH is increased, and the adsorption capacity shows a decreasing tendency when the pH is more than 6,functional groups such as carboxyl, amino and sulfhydryl grafted by FNMs-Cys lose protons, so that the surface of FNMs-Cys is negatively charged, which generates electrostatic interaction with positively charged Pb<sup>2+</sup>, and FNMs-Cys adsorbs lead on deprotonated amino, carboxyl and sulfhydryl through electrostatic interaction [56]. Based on the above analysis, it is speculated that the possible adsorption mechanisms mainly include complex adsorption, electrostatic adsorption and physical adsorption.

#### 4. Conclusion

In this study, a new magnetically responsive porous nanomaterial adsorbent FNMs-Cys was studied for the first time, and the removal efficiency of  $Pb^{2+}$  from aqueous solution was investigated by adsorption. The optimal synthesis conditions of FNMs-Cys were obtained by orthogonal experiments. The results showed that the adsorption capacity of the material is affected by the solution pH, concentration of the metal ions, dosage of adsorbents ,and adsorption material. The optimized pH was 6 a for adsorption of  $Pb^{2+}$  ions, respectively. It was also found that the Langmuir model is the best model to describe adsorption behavior of these ions onto FNMs-Cys. According to Langmuir equation the maximum adsorption values of  $Pb^{2+}$  was 178.57 mg/g respectively. In addition, the kinetic study demonstrated that the adsorption process followed the pseudosecond-order model. Thermodynamic studies also suggested that the adsorption process of aforementioned metal ions onto the FNMs-Cys is endothermic and entropy favored in nature. The results of this study show that FNMs-Cys composite is a kind of adsorbent with good adsorption performance, easy recovery and good regeneration performance, and has good adsorption effect on  $Pb^{2+}$ , and can be used as a magnetic adsorbent material to remove  $Pb^{2+}$ .

#### References

[1] Yang, W.-Y.; Zhang, Z.-Y.; Mujaj, B.; Thijs, L.; Staessen, J. A. Environmental Exposure to Lead: Old Myths Never Die. *Lancet Public Health* 2018. https://doi.org/10.1016/s2468-2667(18)30131-2.

- [2] Mramba, A. S.; Ndibewu, P. P.; Sibali, L. L.; Makgopa, K. A Review on Electrochemical Degradation and Biopolymer Adsorption Treatments for Toxic Compounds in Pharmaceutical Effluents. *ELECTROANALYSIS* 2020, *32* (12), 2615–2634. https://doi.org/10.1002/elan.202060454.
- [3] Bezzina, J.; Robshaw, T.; Dawson, R.; Ogden, M. Single Metal Isotherm Study of the Ion Exchange Removal of Cu(II), Fe(II), Pb (II) and Zn(II) from Synthetic Acetic Acid Leachate. *CHEMICAL ENGINEERING JOURNAL* 2020, 394 (2006-03-01), 1303-1309. https://doi.org/ 10.1016/ j.cej. 2020. 124862.
- [4] Kim, J.; Lee, J. E.; Lee, J.; Yu, J. H.; Kim, B. C.; An, K.; Hwang, Y.; Shin, C.-H.; Park, J.-G.; Kim, J.; Hyeon, T. Magnetic Fluorescent Delivery Vehicle Using Uniform Mesoporous Silica Spheres Embedded with Monodisperse Magnetic and Semiconductor Nanocrystals. *J. Am. Chem. Soc.* 2006. https://doi.org/10.1021/ja0565875.
- [5] Lakic, M.; Breijaert, T. C.; Daniel, G.; Svensson, F. G.; Kessler, V. G.; Seisenbaeva, G. A. Uptake and Separation of Rare Earth Elements and Late Transition Metal Cations by Nanoadsorbent Grafted with Diamino Ligands. *SEPARATION AND PURIFICATION TECHNOLOGY* 2023, *323* (124487). https://doi.org/10.1016/j.seppur.2023.124487.
- [6] Ahmed, M. B.; Zhou, J. L.; Ngo, H. H.; Guo, W.; Chen, M. Progress in the Preparation and Application of Modified Biochar for Improved Contaminant Removal from Water and Wastewater. *Bioresource Technol.* 2016. https://doi.org/10.1016/j.biortech.2016.05.057.
- [7] Sabbarese, C.; Ambrosino, F.; D'Onofrio, A.; Roca, V. Radiological Characterization of Natural Building Materials from the Campania Region (Southern Italy). *Constr. Build. Mater.* 2020. https://doi.org/10.1016/j.conbuildmat.2020.121087.
- [8] Chen, J. H.; Xing, H. T.; Guo, H. X.; Li, G. P.; Weng, W.; Hu, S. R. Preparation, Characterization and Adsorption Properties of a Novel 3-Aminopropyltriethoxysilane Functionalized Sodium Alginate Porous Membrane Adsorbent for Cr(III) Ions. *J. Hazard. Mater.* 2013. https://doi. org/10. 1016/j.jhazmat.2013.01.042.
- [9] Kyzas, G. Z.; Kostoglou, M.; Vassiliou, A. A.; Lazaridis, N. K. Treatment of Real Effluents from Dyeing Reactor: Experimental and Modeling Approach by Adsorption onto Chitosan. *Chem. Eng. J.* 2011. https://doi.org/10.1016/j.cej.2011.01.026.
- [10] Jafari Eskandari, M.; Hasanzadeh, I. Size-Controlled Synthesis of Fe3O4 Magnetic Nanoparticles via an Alternating Magnetic Field and Ultrasonic-Assisted Chemical Co-Precipitation. *Mater. Sci. Eng. B* 2021. https://doi.org/10.1016/j.mseb.2021.115050.
- [11] Ganapathe, L. S.; Mohamed, M. A.; Mohamad Yunus, R.; Berhanuddin, D. D. Magnetite (Fe3O4) Nanoparticles in Biomedical Application: From Synthesis to Surface Functionalisation. *Magnetochemistry* 2020. https://doi.org/10.3390/magnetochemistry6040068.
- [12] Samadi, M. S.; Shokrollahi, H.; Zamanian, A. The Magnetic-Field-Assisted Synthesis of the Co-Ferrite Nanoparticles via Reverse Co-Precipitation and Their Magnetic and Structural Properties. *Mater. Chem. Phys.* 2018. https://doi.org/10.1016/j.matchemphys.2018.05.067.
- [13] Zhao, X.; Li, J.; Cui, X.; Bi, Y.; Han, X. Construction of Novel 3D ZnO Hierarchical Structure with Fe3O4 Assist and Its Enhanced Visible Light Photocatalytic Performance. *J. Environ. Chem. Eng.* 2020. https://doi.org/10.1016/j.jece.2019.103548.
- [14] Chang, Q.; Zhu, L.; Yu, C.; Tang, H. Synthesis and Properties of Magnetic and Luminescent Fe3O4/SiO2/Dye/SiO2 Nanoparticles. *J. Lumin.* 2008. https://doi.org/10.1016/j.jlumin. 2008. 05. 014.
- [15] Zandipak, R.; Sobhanardakani, S. Novel Mesoporous Fe 30 4/SiO 2/CTAB–SiO 2 as an Effective Adsorbent for the Removal of Amoxicillin and Tetracycline from Water. *Clean Techn. Environ. Policy* 2018. https://doi.org/10.1007/s10098-018-1507-5.
- [16] Vojoudi, H.; Badiei, A.; Bahar, S.; Mohammadi Ziarani, G.; Faridbod, F.; Ganjali, M. R. A New Nano-Sorbent for Fast and Efficient Removal of Heavy Metals from Aqueous Solutions Based on Modification of Magnetic Mesoporous Silica Nanospheres. *J. Magn. Magn. Mater.* 2017. https://doi.org/10.1016/j.jmmm.2017.05.065.

- [17] Liu, D.; Pan, J.; Tang, J.; Lian, N. Preparation of Polymethacrylate Monolith Modified with Cysteine for the Determination of Cr(Iii) Ions. *RSC Adv.* 2018. https://doi.org/10.1039/c8ra01287c.
- [18] Fan, H.-L.; Li, L.; Zhou, S.-F.; Liu, Y.-Z. Continuous Preparation of Fe 3 O 4 Nanoparticles Combined with Surface Modification by L -Cysteine and Their Application in Heavy Metal Adsorption. *Ceram. Int.* 2016. https://doi.org/10.1016/j.ceramint.2015.11.098.
- [19] Zou, X.; Yin, Y.; Zhao, Y.; Chen, D.; Dong, S. Synthesis of Ferriferrous Oxide/l-Cysteine Magnetic Microspheres and Their Adsorption Capacity for Pb (II) Ions. *Mater. Lett.* 2015. https://doi.org/10.1016/j.matlet.2015.02.133.
- [20] Abou El-Reash, Y. G. Magnetic Chitosan Modified with Cysteine-Glutaraldehyde as Adsorbent for Removal of Heavy Metals from Water. *J. Environ. Chem. Eng.* 2016. https://doi. org/10. 1016/j.jece.2016.08.014.
- [21] Deng, Y.; Qi, D.; Deng, C.; Zhang, X.; Zhao, D. Superparamagnetic High-Magnetization Microspheres with an Fe3O4@SiO2 Core and Perpendicularly Aligned Mesoporous SiO2 Shell for Removal of Microcystins. *JOURNAL OF THE AMERICAN CHEMICAL SOCIETY* 2008, *130* (1), 28-+. https://doi.org/10.1021/ja0777584.
- [22] Wang, J.; Guo, X. Adsorption Kinetic Models: Physical Meanings, Applications, and Solving Methods. *JOURNAL OF HAZARDOUS MATERIALS* 2020, *390*. https://doi.org/10.1016/j.jhazmat.2020.122156.
- [23] Kilincer, M.; Saygin, H.; Ozyurek, M.; Baysal, A. Sorption of Thiamin (Vitamin B1) onto Micro (Nano)Plastics: pH Dependence and Sorption Models. *J. Environ. Sci. Health Part A* 2023. https://doi.org/10.1080/10934529.2023.2216123.
- [24] O.O. Zhokh; A.I. Trypolskyi; P.E. Strizhak. Discrimination of a Chemical Kinetic Mechanism for Heterogeneously Catalyzed Reactions Using Intraparticle Diffusion. *Chem. Eng. J.* 2023. https://doi.org/10.1016/j.cej.2023.145729.
- [25] Araujo, C. S. T.; Almeida, I. L. S.; Rezende, H. C.; Marcionilio, S. M. L. O.; Leon, J. J. L.; de Matos, T. N. Elucidation of Mechanism Involved in Adsorption of Pb(II) onto Lobeira Fruit (Solanum Lycocarpum) Using Langmuir, Freundlich and Temkin Isotherms. *MICROCHEMICAL JOURNAL* 2018, 137 (2018-02-20), 348-354. https://doi.org/10.1016/j.microc.2017.11.009.
- [26] Hu, Q.; Zhang, Z. Application of Dubinin–Radushkevich Isotherm Model at the Solid/Solution Interface: A Theoretical Analysis. *J. Mol. Liq.* 2019. https://doi.org/10.1016/j.molliq.2019.01.005.
- [27] Fenti, A.; Iovino, P.; Salvestrini, S. Some Remarks on "A Critical Review of the Estimation of the Thermodynamic Parameters on Adsorption Equilibria. Wrong Use of Equilibrium Constant in the Van't Hoof Equation for Calculation of Thermodynamic Parameters of Adsorption" Journal of Molecular Liquids 273 (2019) 425-434. *JOURNAL OF MOLECULAR LIQUIDS* 2019, *276*, 529–530. https://doi.org/10.1016/j.molliq.2018.12.019.
- [28] Ma, J.; Sun, N.; Wang, C.; Xue, J.; Qiang, L. Facile Synthesis of Novel Fe 3 O 4 @SiO 2 @mSiO 2 @TiO 2 Core-Shell Microspheres with Mesoporous Structure and Their Photocatalytic Performance. *J. Alloys Compd.* 2018. https://doi.org/10.1016/j.jallcom.2018.02.005.
- [29] Liu, H.; Ji, S.; Yang, H.; Thang, M. Ultrasonic-Assisted Ultra-Rapid Synthesis of Monodisperse Meso-SiO2@Fe3O4 Microspheres with Enhanced Mesoporous Structure. *Ultrason. Sonochem.* 2013. https://doi.org/10.1016/j.ultsonch.2013.08.010.
- [30] Yang, P.; Huang, S.; Kong, D.; Lin, J.; Fu, H. Luminescence Functionalization of SBA-15 by YVO4:Eu3+ as a Novel Drug Delivery System. *Inorg. Chem.* 2007. https://doi.org/10.1021/ic0622959.
- [31] Huang, J.; Ye, M.; Qu, Y.; Chu, L.; Chen, R.; He, Q.; Xu, D. Pb (II) Removal from Aqueous Media by EDTA-Modified Mesoporous Silica SBA-15. *J. Colloid Interface Sci.* 2012. https://doi.org/10.1016/j.jcis. 2012. 06.054.
- [32] Lee, M.-E.; Park, J. H.; Chung, J. W. Comparison of the Lead and Copper Adsorption Capacities of Plant Source Materials and Their Biochars. *J. Environ. Manag.* 2019. https://doi.org/10.1016/j.jenvman. 2019. 01.100.
- [33] Yang, Y.; Shan, R.; Xiao, Y.; Zhao, F.; Yuan, H.; Chen, Y. Effect of CeO2-Reinforcement on Pb Absorption by Coconut Coir-Derived Magnetic Biochar. *Int. J. Mol. Sci.* 2023. https://doi.org/ 10.3390/ijms24031974.

- [34] Chung, J.; Chun, J.; Lee, S. H.; Lee, Y. J.; Hong, S. W. Sorption of Pb(II) and Cu(II) onto Multi-Amine Grafted Mesoporous Silica Embedded with Nano-Magnetite: Effects of Steric Factors. *J. Hazard. Mater.* 2012. https://doi.org/10.1016/j.jhazmat.2012.08.063.
- [35] Zhang, Y.; Bai, L.; Zhou, W.; Lu, R.; Gao, H.; Zhang, S. Superior Adsorption Capacity of Fe3O4@nSiO2@mSiO2 Core-Shell Microspheres for Removal of Congo Red from Aqueous Solution. *J. Mol. Liq.* 2016. https://doi.org/10.1016/j.molliq.2016.02.096.
- [36] Wu, Q.; Wang, D.; Chen, C.; Peng, C.; Cai, D.; Wu, Z. Fabrication of Fe304/ZIF-8 Nanocomposite for Simultaneous Removal of Copper and Arsenic from Water/Soil/Swine Urine. *J. Environ. Manag.* 2021. https://doi.org/10.1016/j.jenvman.2021.112626.
- [37] Rafigh, S. M.; Heydarinasab, A. Mesoporous Chitosan–SiO2 Nanoparticles: Synthesis, Characterization, and CO2 Adsorption Capacity. *ACS Sustain. Chem. Eng.* 2017. https://doi.org/10.1021/acssuschemeng.7b02388.
- [38] Rafigh, S. M.; Heydarinasab, A. Mesoporous Chitosan–SiO2 Nanoparticles: Synthesis, Characterization, and CO2 Adsorption Capacity. *ACS Sustain. Chem. Eng.* 2017. https://doi.org/10.1021/acssuschemeng.7b02388.
- [39] Nushin Ettekali; Somaiyeh Allahyari; Nader Rahemi; Fahime Abedini. One-Pot Oxidative-Adsorptive Desulfurization of Model and Real Fuel Using Micro-Mesoporous SiO2 Aerogel Supported MoO3. *Micropor. Mesopor. Mater.* 2021. https://doi.org/10.1016/j.micromeso.2021.111376.
- [40] Lu, W.; Lu, H.; Zhang, Z. TiO2-SiO2 Supported MnWO x Catalysts by Liquid-Phase Deposition for Low-Temperature NH3-SCR. *Royal Soc. Open Sci.* 2019. https://doi.org/10.1098/rsos.180669.
- [41] Du, C.; Song, Y.; Shi, S.; Jiang, B.; Yang, J.; Xiao, S. Preparation and Characterization of a Novel Fe3O4-Graphene-Biochar Composite for Crystal Violet Adsorption. *Sci. Total Environ.* 2019. https://doi.org/10.1016/j.scitotenv.2019.134662.
- [42] Lunde, P. J.; Kester, F. L. Chemical and Physical Gas Adsorption in Finite Multimolecular Layers. *Chem. Eng. Sci.* 1975. https://doi.org/10.1016/0009-2509(75)85027-5.
- [43] Heidari, A.; Younesi, H.; Mehraban, Z. Removal of Ni(II), Cd(II), and Pb(II) from a Ternary Aqueous Solution by Amino Functionalized Mesoporous and Nano Mesoporous Silica. *Chem. Eng. J.* 2009. https://doi.org/10.1016/j.cej.2009.06.016.
- [44] Dinh, V.-P.; Le, N.-C.; Tuyen, L. A.; Hung, N. Q.; Nguyen, V.-D.; Nguyen, N.-T. Insight into Adsorption Mechanism of Lead(II) from Aqueous Solution by Chitosan Loaded MnO 2 Nanoparticles. *Mater. Chem. Phys.* 2018. https://doi.org/10.1016/j.matchemphys.2017.12.071.
- [45] Anbia, M.; Lashgari, M. Synthesis of Amino-Modified Ordered Mesoporous Silica as a New Nano Sorbent for the Removal of Chlorophenols from Aqueous Media. *Chem. Eng. J.* 2009. https://doi. org/10.1016/j.cej.2009.02.023.
- [46] Chen, Y.; Yang, Z.; Zhang, Q.; Fu, D.; Chen, P.; Li, R.; Liu, H.; Wang, Y.; Liu, Y.; Lv, W.; Liu, G. Effect of Tartaric Acid on the Adsorption of Pb ( II ) via Humin: Kinetics and Mechanism. *J. Taiwan Inst. Chem. E.* 2020. https://doi.org/10.1016/j.jtice.2019.11.012.
- [47] Repo, E.; Warchoł, J. K.; Bhatnagar, A.; Sillanpää, M. Heavy Metals Adsorption by Novel EDTA-Modified Chitosan–Silica Hybrid Materials. *J. Colloid Interface Sci.* 2011. https://doi.org/10.1016/j.jcis. 2011.02.059.
- [48] Song, Q.; Fang, Y.; Liu, Z.; Li, L.; Wang, Y.; Liang, J.; Huang, Y.; Lin, J.; Hu, L.; Zhang, J.; Tang, C. The Performance of Porous Hexagonal BN in High Adsorption Capacity towards Antibiotics Pollutants from Aqueous Solution. *Chem. Eng. J.* 2017. https://doi.org/10.1016/j.cej.2017.05.057.
- [49] Li, M.; Qin, X.; Cui, J.; Guo, R.; Guo, C.; Wang, Z.; Li, T. Three-Dimensional Electro-Fenton Degradation for Fulvic Acids with Cu-Fe Bimetallic Aerogel-like Carbon as Particle Electrode and Catalyst: Electrode Preparation, Operation Parameter Optimization and Mechanism. *J. Environ. Chem. Eng.* 2021. https://doi.org/10.1016/j.jece.2021.105573.
- [50] Madrid, J. F.; Nuesca, G. M.; Abad, L. V. Amine Functionalized Radiation-Induced Grafted Water Hyacinth Fibers for Pb2+, Cu2+ and Cr3+ Uptake. *Radiat. Phys. Chem.* 2014. https://doi.org/10.1016/j.radphyschem.2013.12.009.

- [51] Beyhan Kocadagistan; Kubra Oksuz. Pb (II) Recovery by Modified Tuffite: Adsorption, Desorption, and Kinetic Study. *Adsorp. Sci. Technol.* 2022. https://doi.org/10.1155/2022/7195777.
- [52] Safri, A.; Fletcher, A. J.; Abdel-Halim, E.; Ismail, M. A.; Hashem, A. Calligonum Crinitum as a Novel Sorbent for Sorption of Pb(II) from Aqueous Solutions: Thermodynamics, Kinetics, and Isotherms. *J. Polym. Environ.* 2020. https://doi.org/10.1007/s10924-020-01975-6.
- [53] Senol-Arslan, D. Isotherms, Kinetics and Thermodynamics of Pb(Ii) Adsorption by Crosslinked Chitosan/Sepiolite Composite. *Polym. Bull.* 2021. https://doi.org/10.1007/s00289-021-03688-9.
- [54] Zhang, F.; Zhu, Z.; Dong, Z.; Cui, Z.; Wang, H.; Hu, W.; Zhao, P.; Wang, P.; Wei, S.; Li, R.; Ma, J. Magnetically Recoverable Facile Nanomaterials: Synthesis, Characterization and Application in Remediation of Heavy Metals. *Microchem. J.* 2011. https://doi.org/10.1016/j.microc.2011.03.005.
- [55] Zhang, W.; Song, J.; He, Q.; Wang, H.; Lyu, W.; Feng, H.; Xiong, W.; Guo, W.; Wu, J.; Chen, L. Novel Pectin Based Composite Hydrogel Derived from Grapefruit Peel for Enhanced Cu(II) Removal. *J. Hazard. Mater.* 2019. https://doi.org/10.1016/j.jhazmat.2019.121445.
- [56] Beagan, A. M. Investigating Methylene Blue Removal from Aqueous Solution by Cysteine-Functionalized Mesoporous Silica. *J. Chem.* 2021. https://doi.org/10.1155/2021/8839864.
- [57] Kandah, M. I.; Meunier, J.-L. Removal of Nickel Ions from Water by Multi-Walled Carbon Nanotubes. *Journal of hazardous materials* 2007, *146* (1–2), 283–288. https://doi.org/ 10.1016/ j.jhazmat. 2006. 12.019.